An adaptive robot controller
design, simulation and implementation

van Gerwen, L.J.W.

Award date:
1990

An adaptive robot controller:

Design, simulation and implementation

L.J.W. van Gerwen

WFW report 90.036

Professor: Dr. ir. J.J. Kok
Coach: Ir. A.G. de Jager

august 1990

Eindhoven University of Technology
Department of Mechanical Engineering
Division of Mechanical Engineering Fundamentals

CONTENTS

SUMMARY

Mechanical manipulators are controlled in order to make their end–effector track a desired trajectory. For this purpose a controller is designed on account of the available information of the system. This information is put into a model, which does not exactly correspond to the actual system. There are always phenomena like measurement noise, unmodelled dynamics and unknown parameters. The level of robustness depends on the influence of these model errors on the control behaviour. A controller is robust, when model errors have little influence on the control behaviour.

In literature many robust controllers are proposed, but only a few are actually applied. Therefore research into practical application of existing controllers is just as important as research into new controllers. The adaptive controller of Slotine and Li (1987) enjoys, according to them, essentially the same level of robustness to unmodelled dynamics as the PD controller, but achieves much better tracking accuracy. This adaptive controller estimates model parameters on–line, so it is attractive to use in the presence of large parameter uncertainties.

The presented research into the adaptive controller consists of three parts:

- o Simulation of a rigid system: The RT–robot
- o Simulation of a flexible system: The XY–table
- o Implementation in the XY–table

Attention is paid to the comparison between the PD and adaptive controller in the presence of modelling errors. Unmodelled dynamics are added to the simulated RT–robot, which are not taken into account for the controller design. Research is done into the modelling errors of the actual XY–table. It is shown that the adaptive controller does not have to have essentially the same level of robustness to unmodelled dynamics as the PD controller. But the implemented adaptive controller achieves much better tracking accuracy in the presence of unmodelled dynamics than the PD controller. The estimated parameters converge to the same values, no matter what the starting parameter values are. Indeed, the adaptive controller of Slotine and Li can be recommended for complex industrial tasks.

NOTATION

A, a	scalar number
|a|	absolute value
a	column (small italic characters)
a_i	i–th term
A	matrix (capital italic characters)
A_{ij}	term on row i, column j
a^T, A^T	transpose
A^{-1}	inverse
$\hat{a}$	estimate
a_d	desired a
$\tilde{a}$	a–a_d (tracking error)
$\dot{a}$	first order time derivative
$\ddot{a}$	second order time derivative
diag(a,b)	diagonal matrix $\begin{bmatrix} a & 0 \\ 0 & b \end{bmatrix}$

CHAPTER 1: INTRODUCTION

Industrial robots are controlled in order to make its end–effector track a desired trajectory. A controller design is based on a model of the system. When this model would completely correspond to the system, a controller using only full dynamics feedforward would cause the desired trajectory to be tracked without tracking errors. In practice the model will never correspond exactly to the system. There will always be some modelling errors:

- The *dynamic structure* may not be known exactly. For example a mechanical manipulator is often considered stiff, while there could be some significant flexibility in the manipulator. Sometimes significant non–linearities are known to be present, but cannot be taken into account in the controller implementation because of the computational effort.

- The dynamic behaviour of a robot also depends on *parameter values.* Parameters are physical properties like inertia, mass, friction, gravitation and geometrical properties like angles and lengths. The parameter values are not always known exactly.

- The controller design is often based on a continuous time model. On–line control takes processing time, which causes *time delay.*

- Measuring instruments have some inaccuracy. A computer executes the on–line control algorithm. Only discrete numbers can be processed. This is not a real modelling error, but is mentioned, because it causes tracking errors.

The influence of these modelling errors on the dynamic behaviour of a system controlled with only full dynamics feedforward would be very large. Such a controller is not robust with respect to model errors.

In literature many robust controllers are proposed, but only a few are actually applied. Therefore research into practical application of existing controllers is just as important as research into new controllers. Research is necessary to investigate their feasibility and to compare their performances. One of the proposed controllers in literature is the adaptive controller of Slotine and Li (1987). The main topic of this report is to compare the performance of the PD and adaptive controller.

In chapter 2 the principles of the adaptive controller are explained.

In chapter 3 simulations of the RT–robot, a rigid manipulator, are presented. A description of the RT–robot is given. Simulations with friction and unmodelled dynamics are presented.

In chapter 4 simulations of the XY–table, a flexible manipulator, are presented. A description of the XY–table is given. The influences of motor and end–effector feedback are discussed. Further the PD and adaptive controller are compared. Finally some discretization effects are discussed.

In chapter 5 the PD and adaptive controller are applied to the actual XY–table. A Kalman observer is designed to reconstruct position and speed one sample ahead. Then there is no influence of time delays due to processing time. All sorts of modelling errors are discussed. The flexibility of the XY–table can be reduced by turning on some screws. In

this way, experiments can be done with a rigid and a flexible system. In both situations the PD and adaptive controller are compared.

In chapter 6 conclusions are drawn based on the results obtained. Recommendations are given for further experiments with and improvements of the XY–table.

CHAPTER 2: ADAPTIVE CONTROLLER

The main topic of this report is to compare the PD and adaptive controller. The adaptive controller consists of a PD feedback and a full dynamics feedforward. The unknown parameters are estimated (adapted) on–line. The choice of the control law and adaptation law are such that the derivative of the manipulator's total energy (Lyapunov function) is smaller or equal to zero. Global asymptotic stability is guaranteed through the use of implicit sliding surfaces. To be able to read this report it is not necessary to understand the adaptive controller completely. The most important things to know are that the PD feedback is defined with matrices K_p and K_d and that the adaptation speed depends among others on the matrix Γ^{-1}. Larger elements of Γ^{-1} lead to quicker adaptation of the estimated parameters. In this report the elements of Γ^{-1} will be called the *adaptation values*. The choices of the matrices K_p, K_d and Γ^{-1} are limited by measurement noise and unmodelled dynamics.

Without any proof (see Slotine and Li, 1987) the control law and the adaptation law are given. In absence of friction and disturbances, the dynamics of an n–link manipulator can be written as:

$$H(q)\ddot{q} + C(q,\dot{q})\dot{q} + g(q) = \tau \tag{2.1}$$

with

q: the n–dimensional column of joint displacements

τ: the n–dimensional column of applied joint torques

$H(q)$: the n×n symmetric positive definite manipulator inertia matrix

$C(q,\dot{q})\dot{q}$: the n–dimensional column of centripetal and Coriolis torques

$g(q)$: the n–dimensional column of gravitational torques.

The control law is defined as:

$$\tau = \hat{H}(q)\ddot{q}_r + \hat{C}(q,\dot{q})\dot{q}_r + \hat{g}(q) - K_d s \tag{2.2}$$

with

$\hat{H}$, $\hat{C}$ and $\hat{g}$: estimates of H, C and g

q_r: virtual reference trajectory with $\dot{q}_r = \dot{q}_d - \Lambda\tilde{q}$, $\ddot{q}_r = \ddot{q}_d - \Lambda\dot{\tilde{q}}$

$q_d(t)$, $\dot{q}_d(t)$, $\ddot{q}_d(t)$: desired trajectory

Λ: symmetric positive definite matrix.

K_d: positive definite matrix

s: measure of tracking accuracy $s = \dot{\tilde{q}} + \Lambda\tilde{q}$

$K_d s$: PD feedback $-K_d s = -K_d\dot{\tilde{q}} - K_d\Lambda\tilde{q} = -K_d\dot{\tilde{q}} - K_p\tilde{q}$ (2.2a)

K_p: symmetric positive definite matrix

Because H, C and g are linear in the parameters, (2.2) can be rewritten as:

$$\tau = Y(q,\dot{q},\dot{q}_r,\ddot{q}_r)\hat{a} - K_d s \tag{2.3}$$

with

$Y = Y(q,\dot{q},\dot{q}_r,\ddot{q}_r)$: n×m matrix

$\hat{a}$: the m–dimensional column of the manipulator parameters

The adaptation law is defined as:

$$\dot{\hat{a}} = -\Gamma^{-1}Y^T(q,\dot{q},\dot{q}_r,\ddot{q}_r)s \tag{2.4}$$

with

Γ: symmetric positive definite m×m matrix

CHAPTER 3: SIMULATION OF RT–ROBOT

3.1 Introduction

The adaptive controller will be applied to a rigid manipulator, a RT–robot. First, the RT–robot will be described. Then the gain matrices of the PD feedback will be determined based on the eigenfrequency and damping factor. The influence of larger adaptation values on the tracking errors will be examined, when there are no unmodelled dynamics. This will be done with and without friction. Finally the PD and adaptive controller will be compared, when there are unmodelled dynamics in the actual system. In that case the adaptation values have to be chosen small enough so that the unmodelled dynamics do not cause instability.

3.2 Description of RT–robot

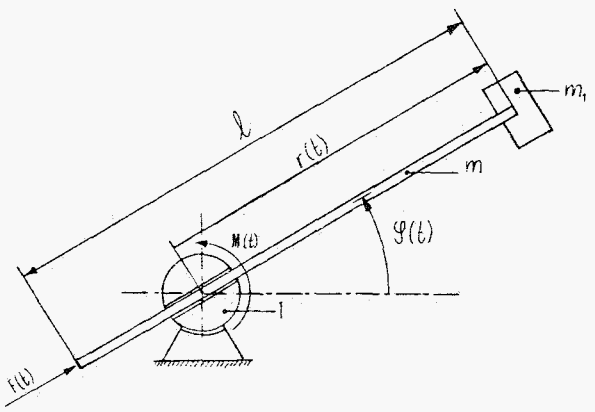

Figure 3.1: RT–robot

In order to compare the PD and adaptive controller, the motion of a simple RT–robot, illustrated in figure 3.1, was simulated.The capitals RT stand for rotation and translation. The RT–robot consists of a disk with moment of inertia I and a rigid bar with length l and homogeneously distributed mass m. If there is no friction, the bar can be pushed up and down inside the disk by force F(t) without any resistance. The load at the end of the bar is a concentrated mass m_1. The disk with bar can be rotated by torque M(t). The system can be described with two degrees of freedom, a rotation $\varphi(t)$ and a translation r(t). The equations of motion, derived with the method of Lagrange, are:

$$P_1\ddot{r} - (P_1 r - P_2)\dot{\varphi}^2 = F$$

$$(P_3 - 2P_2 r + P_1 r^2)\ddot{\varphi} + 2(P_1 r - P_2)\dot{r}\dot{\varphi} = M \qquad (3.1)$$

with parameter values:

$$P_1 = m+m_1 = 15 \text{ [kg]}$$

$$P_2 = \tfrac{1}{2}ml = 5 \text{ [kgm]}$$

$$P_3 = I+\tfrac{1}{3}ml^2 = 8\tfrac{1}{3} \text{ [kgm}^2\text{]}$$

3.3 Gain matrices

The PD and adaptive controller make use of a PD feedback as in equation (2.2a). The gain matrices K_p and K_d influence the eigenfrequencies and damping factors. Larger values of the gain matrices will lead to a quicker response to tracking errors. In practice there will always be measurement noise and unmodelled high–frequency dynamics. Too large values of the gain matrices will lead to less robustness to these effects and could cause instability. At first, simulations will be done without unmodelled high–frequency dynamics. But for the choice of the gain matrices, unmodelled high–frequency dynamics with an eigenfrequency of 25 [rad/s] will already be taken into account. A practical criterion to avoid instability due to these unmodelled dynamics is that the eigenfrequency of the controlled system must be much smaller than the eigenfrequency of the unmodelled dynamics. This is only a practical criterion. Even if the eigenfrequencies are the same, the controlled system could stay stable. Here the eigenfrequency and damping factor are chosen to be:

$$\omega_0 = 10 \text{ [rad/s]}$$

$$\beta = 1 \text{ [–]} \qquad (3.2)$$

With this information the gain matrices can be determined. Linearization of equations (3.1) in a stationary working point (r_0,φ_0) results in:

$$P_1\ddot{r} = F$$

$$I_1\ddot{\varphi} = M \qquad (3.3)$$

$$\text{with } I_1 = (P_3-2P_2r_0+P_1r_0^2)$$

with PD feedback:

$$F = -K_{d1}(\dot{r}-\dot{r}_d) - K_{p1}(r-r_d)$$

$$M = -K_{d2}(\dot{\varphi}-\dot{\varphi}_d) - K_{p2}(\varphi-\varphi_d) \qquad (3.4)$$

Substitution of equations (3.4) in (3.3) makes:

$$\ddot{r} + \frac{K_{d1}}{P_1}\dot{r} + \frac{K_{p1}}{P_1}r = \frac{K_{d1}}{P_1}\dot{r}_d + \frac{K_{p1}}{P_1}r_d$$
$$\ddot{\varphi} + \frac{K_{d2}}{I_1}\dot{\varphi} + \frac{K_{p2}}{I_1}\varphi = \frac{K_{d2}}{I_1}\dot{\varphi}_d + \frac{K_{p2}}{I_1}\varphi_d \qquad (3.5)$$

which can be written as:

$$\ddot{q} + 2\beta\omega_o\dot{q} + \omega_o^2 r = 2\beta\omega_o\dot{r}_d + \omega_o^2 r_d \qquad (3.6)$$

Then the gain matrices are:

$$K_p = \text{diag}(K_{p1},K_{p2}) = \text{diag}(\omega_o^2 P_1,\omega_o^2 I_1)$$
$$K_d = \text{diag}(K_{d1},K_{d2}) = \text{diag}(2\beta\omega_o P_1,2\beta\omega_o I_1) \qquad (3.7)$$

The most unfavourable working point is where the gain matrices are the smallest. Then I_1, which only depends on r_o as shown in equations (3.3), is the smallest. This point, which is the mass centre of the bar with load, because in that point a torque causes the largest acceleration, is:

$$r_o = \tfrac{1}{3}\,[\text{m}] \qquad (3.8)$$

Equations (3.2), (3.7) and (3.8) result in:

$$K_p=\text{diag}(1500,666)$$
$$K_d=\text{diag}(300,133) \qquad (3.9)$$

3.4 Simulation results

The first simulations were done without friction or high–frequency unmodelled dynamics. The desired trajectory in figure 3.2 was:

$$0 \leq t \leq 1.0 \text{ [s]} :$$

$$r_d = \frac{3}{4}t - \frac{3}{8\pi}\sin(2\pi t) + \frac{1}{4} \quad \text{[m]}$$

$$\varphi_d = \frac{\pi}{2}t - \frac{1}{4}\sin(2\pi t) \quad \text{[rad]}$$

$$1.0 \leq t \leq 1.4 \text{ [s]} :$$

$$\dot{r}_d = 0 \; ; \; \dot{\varphi}_d = 0 \qquad (3.10)$$

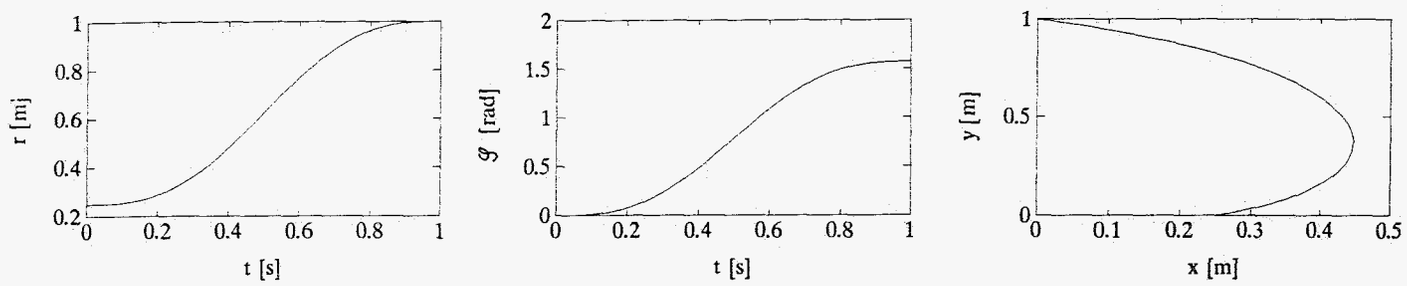

Figure 3.2: Desired trajectory

The design of the adaptive controller is given in appendix A. The initial parameter estimates of the adaptive controller were zero. Then the adaptive controller with adaptation off corresponds to the PD controller. The purpose of the experiments without unmodelled dynamics is not to compare the PD and adaptive controller. For a comparison the bandwidth of the controlled system must be about the same in both cases. Here the adaptation values were increased without looking to the influence on the bandwidth. Later on the adaptation values will be chosen so that the bandwidth does not become larger. Now the only purpose is to watch the tracking errors, when the adaptation values become very large. To do this the maximum absolute tracking errors are compared with different adaptation values. It is clear from figure 3.3 that larger adaptation values lead to smaller tracking errors. In practice there will always be unmodelled dynamics, which will limit the adaptation values. The conclusion is that, when the controller is based on a model with exactly the same structure as the actual system without high–frequency unmodelled dynamics or measurement noise, larger adaptation values lead to smaller tracking errors. When the initial values of the estimated parameters are not zero, but equal to the physical parameters, there will be no tracking errors. When there are no tracking errors, the derivative of the estimated parameters stay zero because of equation (2.4). Then the adaptation values have no influence at all. In figure 3.3 the adaptation value on x–axis means for example:

$$\text{adaptation value} = 10^2 \implies \Gamma^{-1} = \begin{bmatrix} 10^2 & 0 & 0 \\ 0 & 10^2 & 0 \\ 0 & 0 & 10^2 \end{bmatrix}$$

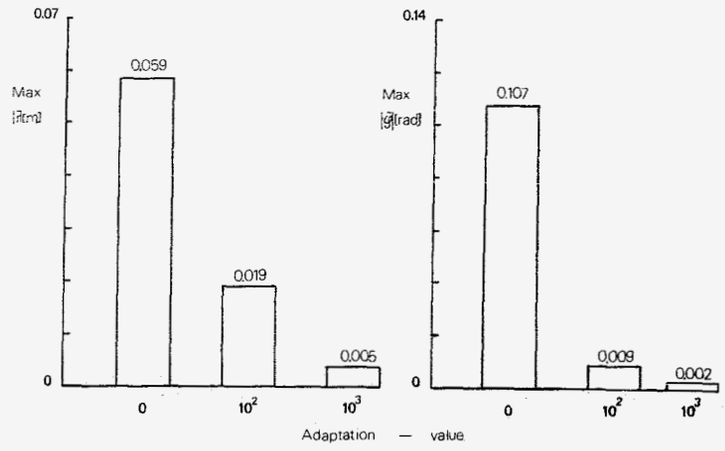

Figure 3.3: Maximum tracking errors

3.5 Friction

In the previous simulations the bar with load could be pushed up and down by force F(t) without any resistance. In practice there will always be friction. In the following simulations with the RT–robot, friction was introduced:

- o Coulomb friction: $P_4 = 20$ [N]
- o viscous friction: $P_5 = 5$ [Ns/m]

The PD controller can be extended with Coulomb friction compensation. Because the exact value of the friction is usually unknown, only fifty percent was compensated. In the adaptive control algorithm it is possible to adapt the friction parameters (see appendix A). The initial values of the parameter estimates were chosen to be zero, except of course the Coulomb friction parameter. The starting value of this parameter was fifty percent of the actual Coulomb friction, just like the compensation term in the PD controller. Again the PD controller corresponds to the adaptive controller with adaptation off. Still there cannot be drawn any conclusion from the comparison between the PD controller and the adaptive controller, for the created bandwidth of the system with adaptive control could be too large with the chosen adaptation values:

$$\Gamma^{-1} = \text{diag}(10^2, 10^2, 10^2, 5.10^2, 5.10^2) \qquad (3.11)$$

The maximum tracking errors in figure 3.4 with adaptation on are the same as the maximum tracking errors in figure 3.3 with adaptation values:

$$\Gamma^{-1} = \text{diag}(10^2, 10^2, 10^2)$$

The added friction does not have significant influence on the maximum tracking errors of the adaptive controller. The adaptive controller compensates the friction well.

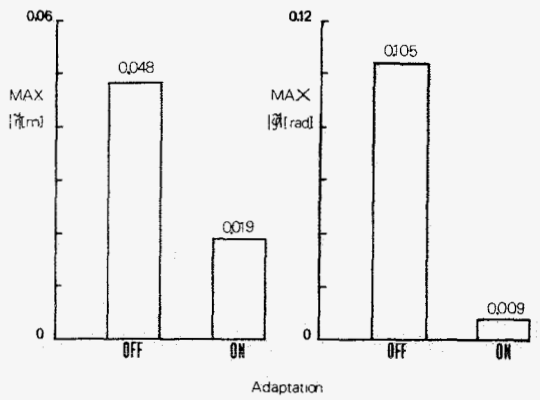

Figure 3.4: Maximum tracking errors

3.6 Unmodelled dynamics

So far the adaptation values could be chosen as large as possible, because the adaptive controller was based on a model with the same structure as the actual system. Now unmodelled dynamics will be added. Dynamics of amplifiers and motors are often neglected in the model. The motor, which applies torque M to the disk of the RT–robot, could for example have its own dynamics. The controller calculates a torque that has to be applied to the disk to track the desired path. The applied torque will not have exactly the same value as the calculated torque. When the calculated torque varies slowly with respect to time, the motor will not have any trouble with applying this torque. But when the calculated torque varies more quickly, the amplitude ratio will decrease and the phase lag will increase. This motor behaviour can be described with a second order system:

$$\ddot{y} + 2\beta\omega_0 \dot{y} + \omega_0^2 y = \omega_0^2 u$$

$$\omega_0 = 25 \text{ [rad/s]}$$

$$\beta = \tfrac{1}{2}\sqrt{2} \text{ [–]} \qquad (3.12)$$

u : calculated torque as input [Nm]
y : applied torque as output [Nm]
β : damping factor of motor [–]
ω_0 : eigenfrequency of motor [rad/s]

The gain matrices of the PD feedback were chosen such that the eigenfrequencies of the RT–robot without motor dynamics were 10 [rad/s]. When the eigenfrequency of the motor dynamics is 25 [rad/s], the system will not become unstable. However, if the eigenfrequency of the motor dynamics is 10 [rad/s], the system will probably become unstable. The adaptation values of the adaptive controller cannot be chosen as large as possible anymore. Too large adaptation values will cause instability. In appendix B adaptation values are determined, which will not cause instability, when the eigenfrequency of the motor dynamics is 25 [rad/s]. The result is:

$$\Gamma^{-1} = \begin{bmatrix} 3 & 0 & 0 & 0 & 0 \\ 0 & 3 & 0 & 0 & 0 \\ 0 & 0 & 3 & 0 & 0 \\ 0 & 0 & 0 & 500 & 0 \\ 0 & 0 & 0 & 0 & 500 \end{bmatrix} \tag{3.13}$$

The simulations, which were done with friction and unmodelled dynamics with $\omega_0 = 10$ [rad/s], showed instability with PD and adaptive controller. The next simulations were done with friction and unmodelled dynamics with $\omega_0 = 25$ [rad/s]. The following situations were simulated:

1: PD controller:

fifty percent Coulomb friction compensation

2: adaptive controller:

initial value of Coulomb friction fifty percent,
initial value of other parameters zero percent

3: adaptive controller:

initial value of Coulomb friction fifty percent,
initial value of other parameters seventy percent

The tracking errors are shown in figure 3.5. The adaptive controller achieves a better tracking accuracy than the PD controller. The parameter estimates of the adaptive controller did not go to their exact values, because the adaptation time was too short and because there were unmodelled dynamics. If the same trajectory had been tracked twice, there would have been more time to adapt the parameter estimates. The adaptation values were chosen small enough not to increase the bandwidth of the controlled system. But for smooth convergence it would be better to chose these values such that the extra poles due to the adaptation and the influence on the existing poles are small. Then, for example, it would not be possible to estimate a part of the mass as a time dependent friction.

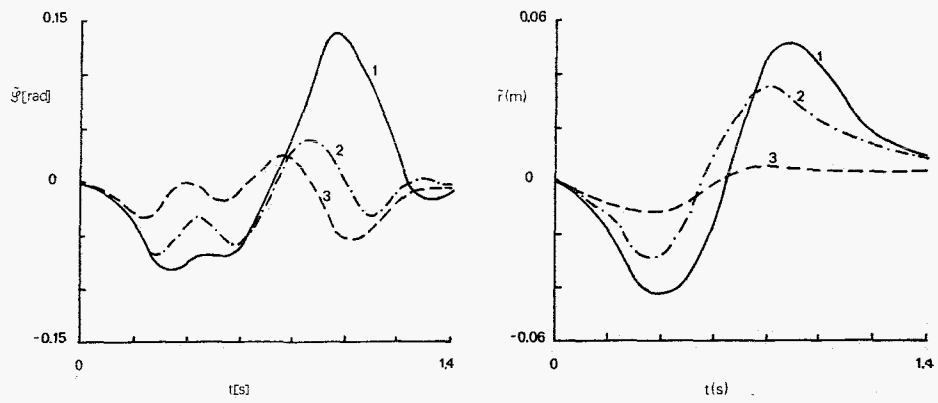

Figure 3.5: Tracking errors

3.7 Conclusion

The adaptive controller achieves better tracking accuracy than the PD controller in case of the simple RT–robot. When there are no unmodelled dynamics, larger adaptation values result in smaller tracking errors. Adding friction is no problem. When there are unmodelled dynamics, the parameters will not converge to their exact values. Another reason, why the parameters did not converge to their exact values, was that the adaptation time was too short. The simulation results of the rigid RT–robot show that it could be useful to apply the adaptive controller to the flexible XY–table.

CHAPTER 4: SIMULATION OF XY–TABLE

4.1 Introduction

The PD and adaptive controller will be applied to the XY–table, which is not rigid like the RT–robot. A description of the XY–table and the equations of motion will be given. The gain matrices will be determined based on the eigenfrequencies and damping factors. Feedback of the end–effector position will give other results than only motor feedback. The influence of different weighing factors for motor and end–effector feedback on the tracking errors will be studied. Next, the simulation results of PD and adaptive controller will be shown. Finally, some discretization effects are discussed.

4.2 Description of XY–table

A top view and a schematic representation of the XY–table are depicted in figure 4.1. The system, used for the simulations, is shown in figure 4.2. Notice the difference of the positive Y–direction between figure 4.1 and figure 4.2. The end–effector is a slide with mass m_e that can move in a horizontal plane by means of three slideways. The couples T_1 and T_3 are applied by two servomotors. There are three degrees of freedom, the rotations $\varphi_1(t)$, $\varphi_2(t)$ and $\varphi_3(t)$. The rotations $\varphi_1(t)$ and $\varphi_2(t)$ differ because of the torsion spring with stiffness k. Coulomb friction is modelled for movements along the three slideways. This friction is represented by the torques W_1, W_2 and W_3. The equations of motion and the exact values of the parameters of the simulated system are given in appendix B. A simple model of this system will be used for designing the PD and adaptive controller. In this model the torsion spring is neglected. Because the rotations $\varphi_1(t)$ and $\varphi_2(t)$ of the simplified model are equal, the model has only two degrees of freedom. The equations of motion of this model, derived in appendix C, are:

$$P_1 \ddot{\varphi}_1 = T_1 - P_3 \operatorname{sign}(\dot{\varphi}_1)$$
$$P_2 \ddot{\varphi}_3 = T_3 - P_4 \operatorname{sign}(\dot{\varphi}_3) \qquad (4.1)$$

with parameter values:

$$P_1 = 2{,}34.10^{-3} \text{ [kgm}^2\text{]}$$
$$P_2 = 2{,}80.10^{-4} \text{ [kgm}^2\text{]}$$
$$P_3 = 0{,}40 \text{ [Nm]}$$
$$P_4 = 0{,}02 \text{ [Nm]} \qquad (4.2)$$

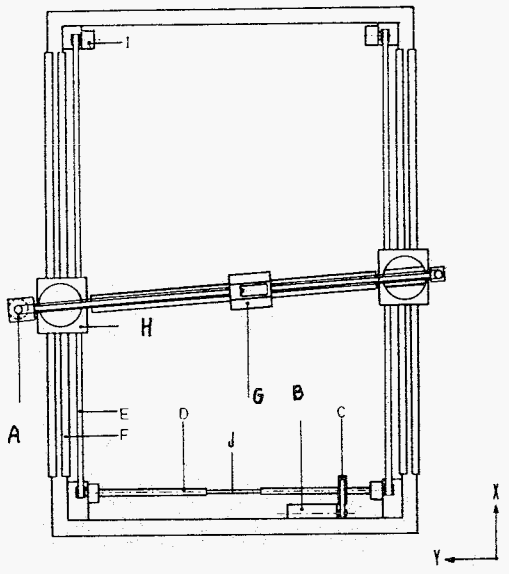

A : Y–motor
B : X–motor
C : transmission
J : TORSION SPRING
D : spindle
E : belt
F : slideway
G : Y–slide
H : X–slide
I : belt wheel

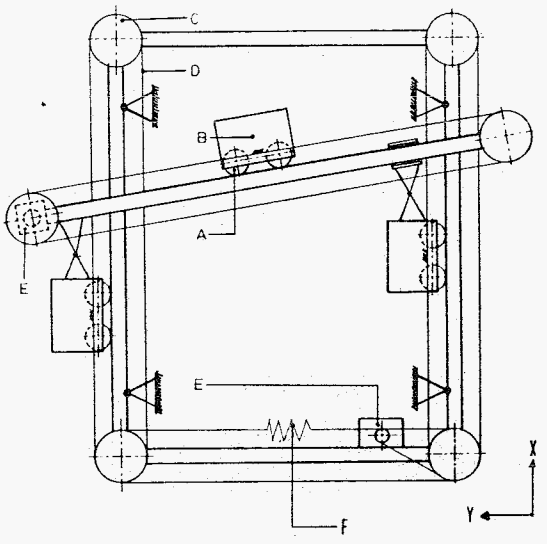

A : slide wheel
B : slide
C : belt wheel
D : belt
E : motors
F : SPRING

Figure 4.1: XY–table

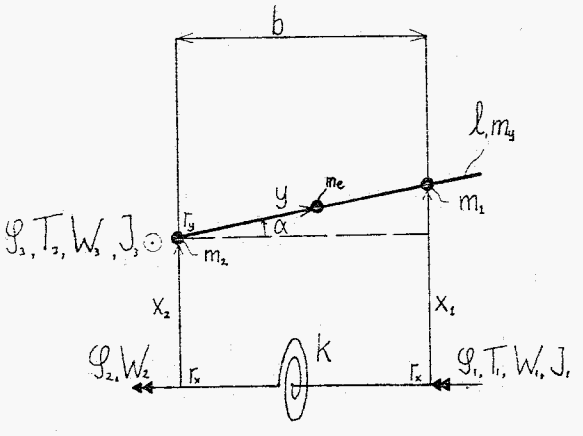

Figure 4.2: Simulated system

4.3 Gain matrices

Equations (4.1) without friction, representing the reduced model, will be used to determine the gain matrices of the PD feedback. The gain matrices can be written as a function of the eigenfrequencies and damping factors.

Model without friction:

$$\begin{aligned} P_1 \ddot{\varphi}_1 &= T_1 \\ P_2 \ddot{\varphi}_3 &= T_3 \end{aligned} \tag{4.3}$$

PD feedback of motor rotations:

$$\begin{aligned} T_1 &= -K_{d1}(\dot{\varphi}_1 - \dot{\varphi}_{1d}) - K_{p1}(\varphi_1 - \varphi_{1d}) \\ T_3 &= -K_{d3}(\dot{\varphi}_3 - \dot{\varphi}_{3d}) - K_{p3}(\varphi_3 - \varphi_{3d}) \end{aligned} \tag{4.4}$$

Substitution of equations (4.4) in (4.3) results in:

$$\begin{aligned} \ddot{\varphi}_1 + \frac{K_{d1}}{P_1}\dot{\varphi}_1 + \frac{K_{p1}}{P_1}\varphi_1 &= \frac{K_{d1}}{P_1}\dot{\varphi}_{1d} + \frac{K_{p1}}{P_1}\varphi_{1d} \\ \ddot{\varphi}_3 + \frac{K_{d3}}{P_2}\dot{\varphi}_3 + \frac{K_{p3}}{P_2}\varphi_3 &= \frac{K_{d3}}{P_2}\dot{\varphi}_{3d} + \frac{K_{p3}}{P_2}\varphi_{3d} \end{aligned} \tag{4.5}$$

This can be written as:

$$\ddot{\varphi} + 2\beta\omega_0\dot{\varphi} + \omega_0^2\varphi = 2\beta\omega_0\dot{\varphi}_d + \omega_0^2\varphi_d \tag{4.6}$$

For simplicity the eigenfrequencies and damping factors are chosen equal for both equations (4.5). This yields:

$$\begin{aligned} K_p &= \mathrm{diag}(K_{p1},K_{p3}) = \mathrm{diag}(\omega_0^2 P_1, \omega_0^2 P_2) \\ K_d &= \mathrm{diag}(K_{d1},K_{d3}) = \mathrm{diag}(2\beta\omega_0 P_1, 2\beta\omega_0 P_2) \end{aligned} \tag{4.7}$$

The choice of the eigenfrequency depends on the unmodelled torsion spring, which could cause instability. To find out how large the eigenfrequency could be chosen, some simulations were done. These simulations were carried out for the system with three degrees of freedom with only motor feedback and no end–effector feedback. The desired trajectory of the end–effector in figure 4.3 was:

$$x_g = t - \frac{1}{2\pi}\sin(2\pi t)$$
$$y_g = t - \frac{1}{2\pi}\sin(2\pi t)$$
$$0 \leq t \leq 1 \text{ [s]} \qquad (4.8)$$

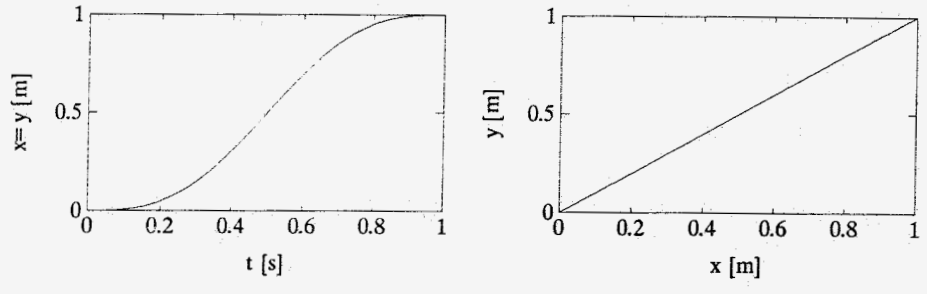

Figure 4.3: Desired trajectory

The tracking errors of the end–effector of simulations with eigenfrequency 10, 50 and 250 [rad/s] and damping factor 1 are shown in figure 4.4. There is not much difference between 50 [Hz] and 250 [Hz], because the motor rotations are following the desired path very well. The largest part of the tracking errors are caused by the deformation of the torsion spring. Because torque T_1 will stay about the same magnitude at higher eigenfrequencies, the deformation will stay the same. The unmodelled torsion spring causes large tracking errors of the end–effector in X–direction, but will never lead to instability. Because simulations with lower eigenfrequencies take less time, the eigenfrequency and damping factor are chosen as follows:

$$\omega_0 = 10 \text{ [rad/s]}$$
$$\beta = 1 \text{ [–]} \qquad (4.9)$$

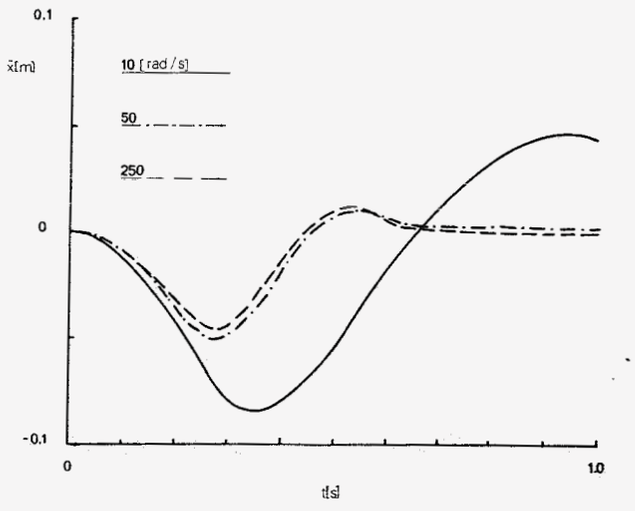

Figure 4.4: Tracking errors of end–effector

4.4 Feedback of motor and end–effector

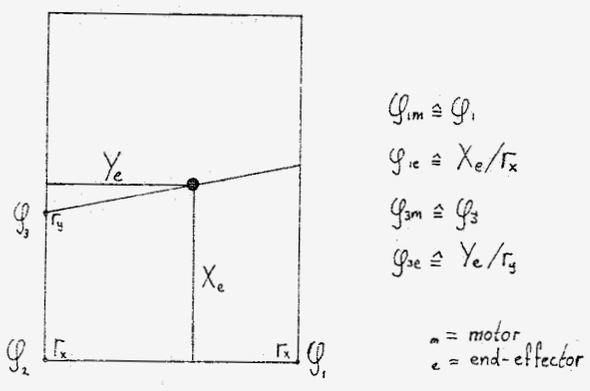

Figure 4.5: Motor and end–effector coördinates

So far, only the rotations and angular speeds of the servomotors have been measured. It is also possible to measure the displacement and speed of the end–effector. The displacement of the end–effector can be written as a rotation by dividing the displacement by the radius

of the belt wheels. This is illustrated in figure 4.5. Weighing factors W_m and W_e can be attached to motor and end–effector. The weighed rotations are now:

$$\varphi_{1w} = \frac{W_m\varphi_{1m} + W_e\varphi_{1e}}{W_m + W_e}$$
$$\varphi_{3w} = \frac{W_m\varphi_{3m} + W_e\varphi_{3e}}{W_m + W_e} \qquad (4.10)$$

If it is desired, more flexibility can be achieved by designing separate end–effector and motor feedback controllers and applying a weighed sum of their respective outputs.
The weighing of the angular speeds goes exactly the same way as in equations (4.10):

$$\dot{\varphi}_{1w} = \frac{W_m\dot{\varphi}_{1m} + W_e\dot{\varphi}_{1e}}{W_m + W_e}$$
$$\dot{\varphi}_{3w} = \frac{W_m\dot{\varphi}_{3m} + W_e\dot{\varphi}_{3e}}{W_m + W_e} \qquad (4.11)$$

The XY–table without friction was controlled in order to make its end–effector track the desired path of equations (4.8). The controller was a PD feedback with gain matrices in form of equations (4.7) with eigenfrequency and damping factor as in equations (4.9). Results of simulations with different weighing factors are shown in figure 4.6. The X–direction is the most sensitive to the weighing factors. The smallest maximum tracking error in X–direction occurs, when the feedback consists of forty percent motor feedback and sixty percent end–effector feedback. When not the maximum of the tracking errors, but the sum of the tracking errors was considered, the optimum could have been a little bit different. But that is not the point here. The conclusion is that only end–effector feedback causes instability, which can be avoided by adding some motor feedback. It would be possible to find the optimum combination of gain matrices and weighing factors by doing a lot of simulations, but it is not the purpose to tune the system. The purpose is to make an honest comparison between PD and adaptive controller.

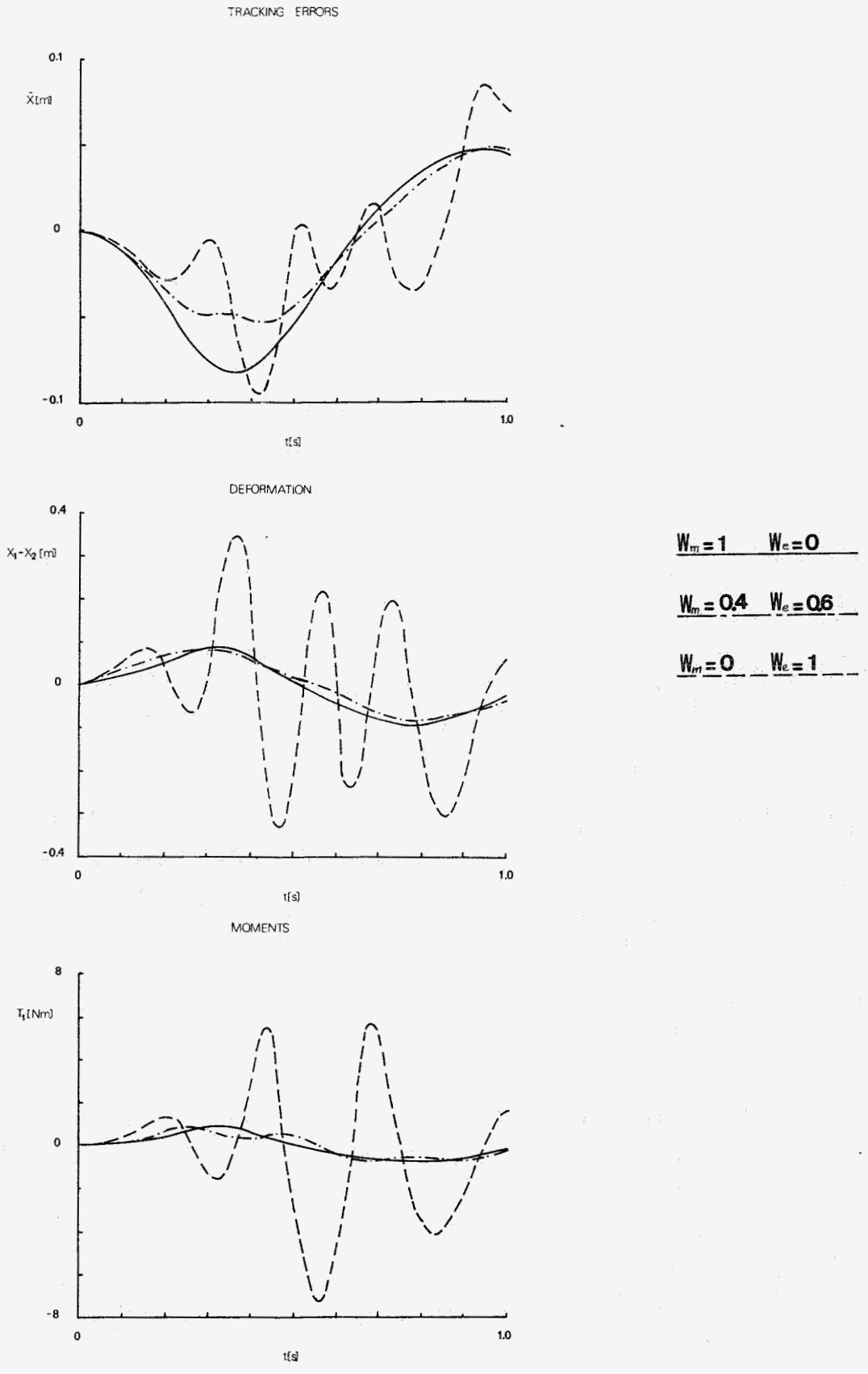

Figure 4.6: Simulation results for different weighing factors

4.5 Simulation results

The XY–table with friction was simulated with PD and adaptive control. The PD feedback for both controllers was as in equations (4.7) and (4.9). There was forty percent motor feedback and sixty percent end-effector feedback. The desired trajectory was not chosen as in equations (4.8), but was chosen to be a circle:

$$x_d = 0{,}5 - 0{,}25\cos(2\pi t)$$

$$y_d = 0{,}5 + 0{,}25\sin(2\pi t)$$

$$x_d, y_d \text{ in [m]} \qquad (4.12)$$

Because the trajectory, which was used to determine the optimal weighing factors, was not this circle, the weighing does not have to be optimal. This does not matter, because it is not the intention to tune this system. The intention is to make a comparison between the PD and adaptive controller. The adaptive controller design is given in appendix D. The adaptation values were chosen as (see appendix D):

$$\Gamma^{-1} = \text{diag}(2.5\cdot 10^{-7}, 2.5\cdot 10^{-8}, 1\cdot 10^{-1}, 1\cdot 10^{-2}) \qquad (4.13)$$

In figure 4.7 the tracking errors are plotted for three different situations:

1: PD controller

2: adaptive controller starting from zero estimates

3: adaptive controller with hundred percent parameters

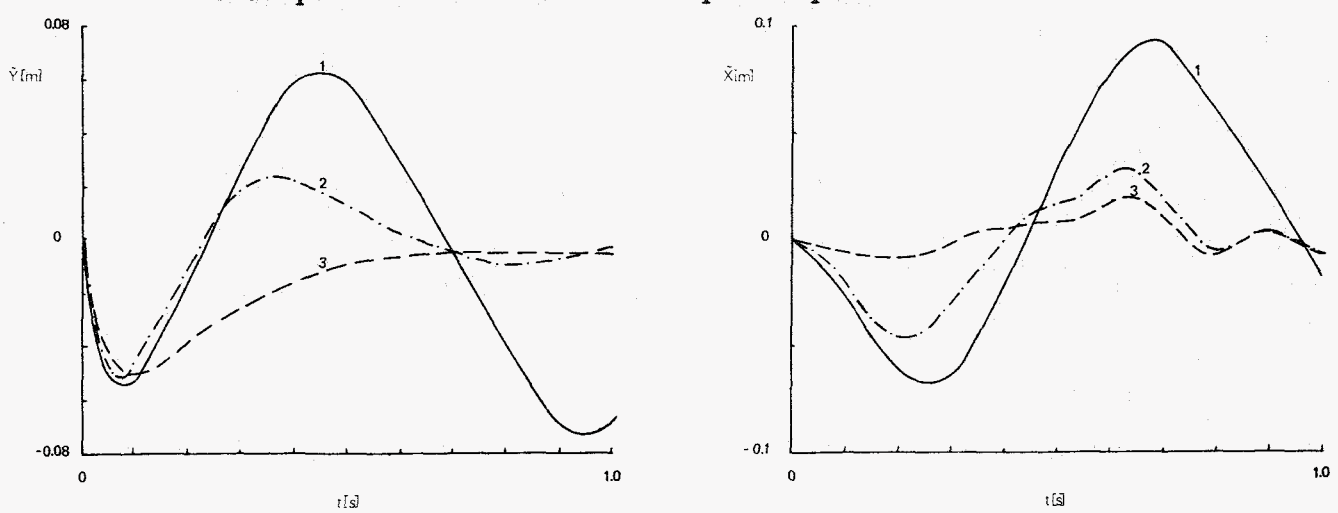

Figure 4.7: Tracking errors of end–effector

In the beginning the tracking errors of PD controller and adaptive controller starting with zero estimates are very close. This was expected, because the adaptive controller with zero parameters and the PD controller are exactly the same. But the parameter estimates in figure 4.8 are quickly driven by the tracking errors. At the end the parameter estimates are so good, that the tracking errors of the adaptive controller starting with zero estimates are very close to the tracking errors of the adaptive controller with hundred percent parameters. The tracking errors of the adaptive controller with hundred percent parameters are not zero, because of the influence of the unmodelled torsion spring and the initial condition in Y–direction. The initial speed in Y–direction was chosen to be zero. But in equations (4.12) the desired initial speed is not zero. In practice there will always be some knowledge of the parameter values. Then the feasible result will lie between the adaptive controller with zero and hundred percent parameters.

In paragraph 4.2 it was shown that higher eigenfrequencies did not cause instability. When the adaptation values are chosen too large, no instabilities will follow. Therefore it could be possible that the adaptation values are too large without noticing. This does not mean that the results are not useful for comparison between PD and adaptive controller. When the adaptation values were chosen smaller, the parameter estimates would have gone more slowly to their final values. In practice it could be possible to make the end-effector track the same circle more than once. After a while, even with much lower adaptation values, the tracking errors of the adaptive controller starting with zero estimates would come very close to the tracking errors of the adaptive controller with hundred percent parameters.

The adaptive controller achieves much better tracking accuracy than the PD controller, even when the model used for the control design is not the same as the actual model. In this case due to the flexibility of the torsion spring.

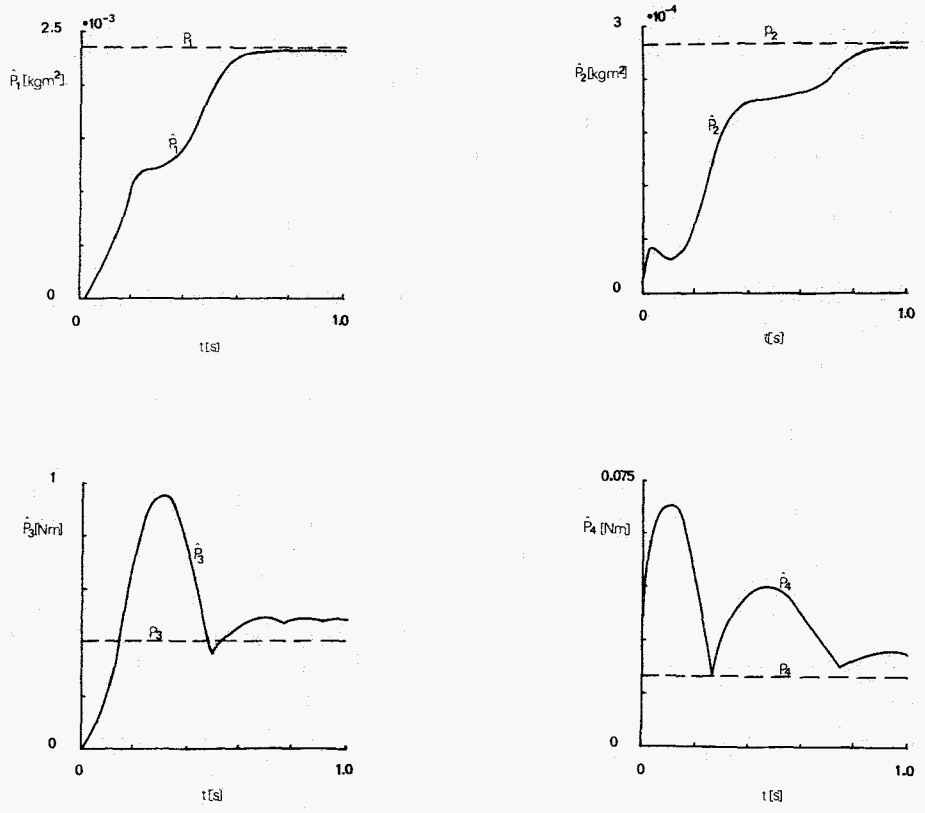

Figure 4.8: Parameter estimates

4.6 Discretization effects

In the above simulations the controllers were continuous with respect to time. In practice a computer executes the on–line control algorithm. This takes processing time and only discrete numbers can be processed. A common practical criterion for a good controller performance, as far as the time delay is concerned: the controller sampling frequency must be at least ten times larger than the maximum response frequency. Undesirable effects of the time delay can be canceled by estimating position and speed one sample ahead. This can be done by means of the well known Kalman observer. Assuming that this Kalman filter will be used in the practical implementation, the time delay does not have to be reckoned with. Then the sampling frequency must be at least a factor 2 to 4 larger than the maximum response frequency to enable detection of this maximum response frequency. In appendix D can be seen, that the largest eigenfrequency of the linearized system with PD and adaptive controller is about 3.4 [Hz]. This means that the sampling frequency must be at least 7 to 14 [Hz]. Simulations were done with the adaptive controller starting with zero parameters, assuming that measuring the output and calculating and applying the input did not take any time. The only effect of sampling was that the computed input and estimated parameters kept the same value during one sampling period. The tracking errors are shown in figure 4.9. The tracking errors at a sampling frequency of 100 [Hz] do not differ much from the continuous controller. At 20 [Hz] the tracking errors are different, but not worse. At 10 [Hz] the system is unstable. From this can be concluded, that for a good performance, even when there is no time delay and no measurement noise, the sampling frequency should be chosen as far as possible above the largest eigenfrequency of the controlled system.

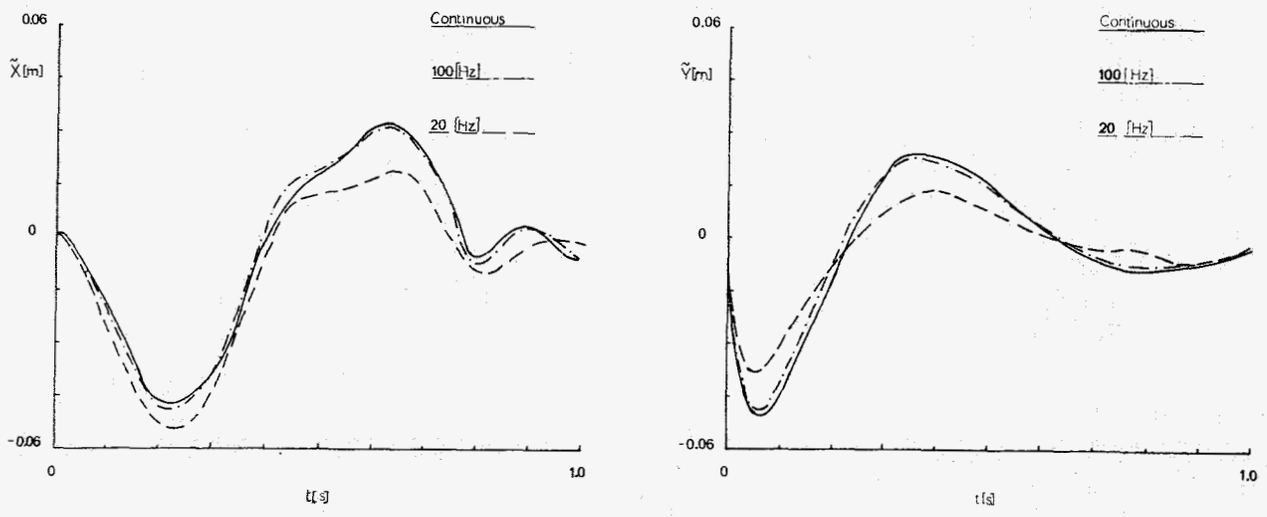

Figure 4.9: Tracking errors at different sampling frequencies

4.7 Conclusion

Instability due to the unmodelled torsion spring can be avoided by adding motor feedback instead of only end–effector feedback. It is possible to tune the XY–table by finding the optimum combination of gain matrices and weighing factors, but this is not the purpose of this report. The purpose is to compare the PD and adaptive controller in the presence of unmodelled dynamics. The adaptive controller achieves much better tracking accuracy than the PD controller. The parameters, especially the mass parameters, are estimated well. The results are promising for implementation of the adaptive controller.

CHAPTER 5: IMPLEMENTATION IN XY–TABLE

5.1 Introduction

The results of chapter 3 and 4 show that it could be very useful to apply the adaptive controller to the actual XY–table. First, a description is given of the XY–table. A Kalman observer will be designed to avoid time delays and discretization effects. Next, all kinds of modelling errors will be discussed. Which of them causes instability and at which eigenfrequency. Experiments will be done with and without the flexible torsion spring.

5.2 Description of XY–table

The XY–table has already been described in chapter 4. The controller hardware is described in Heeren (1989). With the existing hardware and software it was not possible to work with different sampling frequencies. For this purpose a programmable interval timer of type 8253 (Intel) has been added. The software has been adjusted such that the interval timer is programmed automatically by stating the desired sampling frequency. Normally it is possible to measure the servomotor rotations and the end-effector position. Unfortunately, the optical measurement system, which measures the end-effector position, was broken during this study. In contrast with chapter 4 the tracking errors in this chapter relate to the motor rotations and not to the end–effector. There is only motor feedback. The positive Y–direction is different too. This is not so important, but is only mentioned for the sake of completeness and to avoid confusion. Again a simple model is used to design the PD and adaptive controller. The equations of motion, not with torques as in equations (4.1) but with forces, are:

$$\begin{aligned} P_1 \ddot{x} &= F_1 - P_3 \,\mathrm{sign}(\dot{x}) \\ P_2 \ddot{y} &= F_3 - P_4 \,\mathrm{sign}(\dot{y}) \end{aligned} \qquad (5.1)$$

with parameter values:

$$\begin{aligned} P_1 &= 46.5 \text{ [kg]} \\ P_2 &= 4.3 \text{ [kg]} \\ P_3 &= 50.0 \text{ [N]} \\ P_4 &= 15.0 \text{ [N]} \end{aligned} \qquad (5.2)$$

These parameter values are, apart from the transmission between torques and forces, different from equations (4.2), because there was no good information about the parameter values during the simulations of chapter 4. The parameter values of equations (5.2) will also not correspond to the exact parameter values, but this was the best information available during this study.

5.3 Kalman observer

The servomotor rotations are measured with incremental encoders. One possibility to determine the angular speeds is simple numerical differentiation of the servomotor rotations. Differentiation leads to two kinds of errors. First, measurement errors of the rotations cause errors at the size of the differentiation step divided by the time interval. A larger time interval will produce smaller errors due to measuring errors. Secondly, differentiation gives an estimate of the angular speed at the point of time in the middle of the interval, not at the end of the interval. This causes a time delay in the determined angular speed at the size of half a time interval. A larger time interval will produce larger errors due to time delay. These two kinds of errors show that there must be an optimum differentiation interval.

Further, when the motor rotations are measured and the angular speeds are determined by differentiation, the computer has to calculate the inputs to make the end–effector track some desired path. This causes a time delay with respect to the inputs.

The above effects can be reduced by a Kalman observer. The Kalman observer determines the speed not only with the measured rotations like the difference method, but also with the knowledge of the dynamics. Therefore the measurement errors have less influence. The Kalman observer estimates position and speed one sample ahead, using the last estimates, the last measured position, the last calculated forces and the knowledge about the dynamics of the XY–table. The computer calculates the input with the estimated position and speed. The calculated input is applied at the point of time, at which position and speed have been estimated. In this way the time delay can be neglected. The design of the Kalman observer is shown in appendix E. This design is based on a discrete time model, at which a variable sampling frequency has been reckoned with.

5.4 Stability analysis of rigid system

It is possible to change the flexible bar into a rigid bar simply by turning on some screws. Then the simple model, that will be used for the controller design, should structurally be the same as the system. But there are modelling errors (some of them can be detected by looking at the XY–table and pushing the end–effector up and down), which influence the control behaviour:

Moving the end–effector in X– and Y–direction very slowly does not constantly needs the same effort. There are some bad bearings. This causes an harmonic friction term in X– and Y–direction.

There is backlash in one of the bearings in X–direction. When the motor shaft starts moving in an other direction, only one of the two X–slides moves. Then the effective mass is smaller.

The transmissions between motors and slides consist of belts and little springs. These belts can be considered stiff. The little springs can be pushed in very easily. This causes extra flexibility

The belts often touch the sides of the belt wheels, through which the friction changes. This happens in X– and Y–direction.

The XY–table is supported by a concrete block, which could cause vibrations.

Motors and amplifier have been modelled as constant gains, while they have dynamics of their own. The gain factor does not seem to be correct, for the calculated and measured current are not the same. But this only influences the parameter estimates. It does not influence the performance.

Measurement noise. The measured motor rotations are only known in discrete numbers.

Sampling frequency.

Due to this kind of unmodelled dynamics, the PD feedback cannot be chosen too large. To find out which gain matrices cause instability and why, they are written as function of eigenfrequencies and damping factors. The motor rotations are converted into x– and y–coördinates. The PD feedback is then:

$$\begin{aligned} F_1 &= -K_{d1}(\dot{x}-\dot{x}_d) - K_{p1}(x-x_d) \\ F_3 &= -K_{d3}(\dot{y}-\dot{y}_d) - K_{p3}(y-y_d) \end{aligned} \tag{5.3}$$

Substitution of equations (5.3) in (5.1) results in:

$$\begin{aligned} \ddot{x} + \frac{K_{d1}}{P_1}\dot{x} + \frac{K_{p1}}{P_1}x &= \frac{K_{d1}}{P_1}\dot{x}_d + \frac{K_{p1}}{P_1}x_d \\ \ddot{y} + \frac{K_{d3}}{P_2}\dot{y} + \frac{K_{p3}}{P_2}y &= \frac{K_{d3}}{P_2}\dot{y}_d + \frac{K_{p3}}{P_2}y_d \end{aligned} \tag{5.4}$$

This can be written as:

$$\begin{aligned} \ddot{x} + 2\beta_x\omega_{ox}\dot{x} + \omega_{ox}^2 x &= 2\beta_x\omega_{ox}\dot{x}_d + \omega_{ox}^2 x_d \\ \ddot{y} + 2\beta_y\omega_{oy}\dot{y} + \omega_{oy}^2 y &= 2\beta_y\omega_{oy}\dot{y}_d + \omega_{oy}^2 y_d \end{aligned} \tag{5.5}$$

This yields:

$$K_p = \text{diag}(K_{p1}, K_{p3}) = \text{diag}(\omega_{0x}^2 P_1, \omega_{0y}^2 P_2)$$
$$K_d = \text{diag}(K_{d1}, K_{d3}) = \text{diag}(2\beta_x \omega_{0x} P_1, 2\beta_y \omega_{0y} P_2) \qquad (5.6)$$

The first experiments were done in X–direction with a sampling frequency of 133 [Hz] and with desired trajectory:

$$x_d = M - R\cos(2\pi f t),\ y_d = 800$$
$$M = 800\ [\text{mm}],\ R = 150\ [\text{mm}],\ f = \frac{2}{3.75}\ [\text{Hz}]$$
$$0 \leq t \leq 3.75\ [\text{s}] \qquad (5.7)$$

The applied forces in X–direction of experiments with:

$$\omega_{ox} = 5{\times}2\pi\ [\text{rad/s}] \hat{=} 5\ [\text{Hz}],\ \beta_x = 1$$
$$\omega_{ox} = 10{\times}2\pi\ [\text{rad/s}] \hat{=} 10\ [\text{Hz}]\ \beta_x = 1 \qquad (5.8)$$

are shown in figure 5.1.

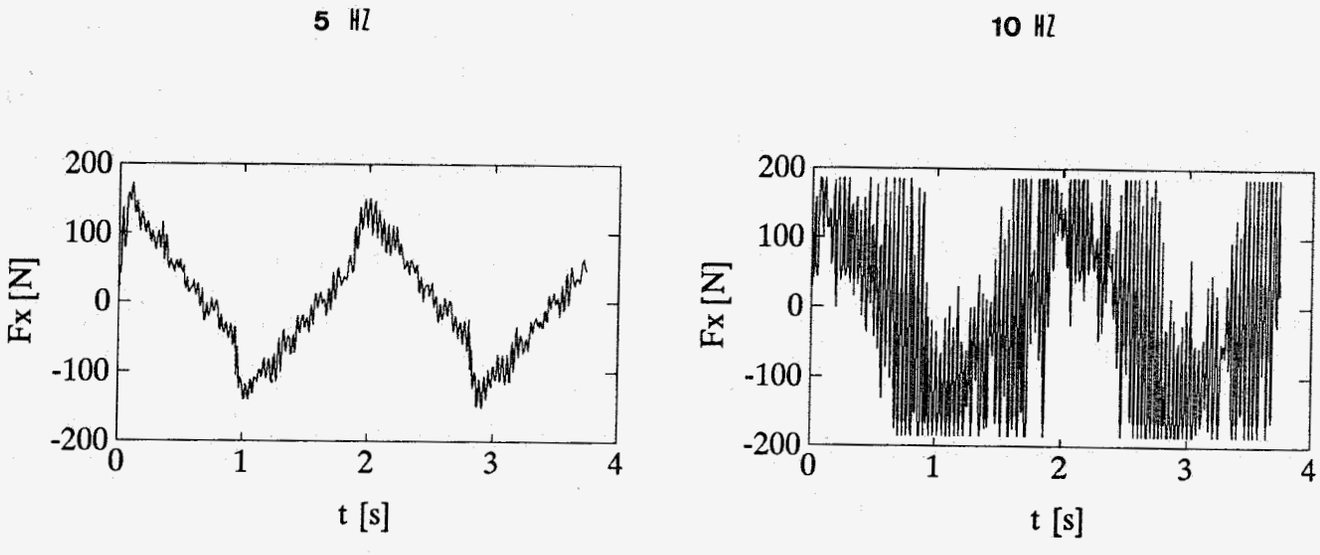

Figure 5.1: Applied forces to total system

At 5 [Hz] little high frequency vibrations arise in the speed errors and the input force. At 10 [Hz] the tracking errors are smaller than at 5 [Hz], but the XY–table shows a chattering response. (The maximum force of about 180 [N] has been built in into the software for safety.) Apparently something causes high frequency vibrations at about 5 [Hz], which leads to undesirable chattering at higher frequencies. To find out whether these vibrations are caused by dynamics of the XY–table itself, like the concrete block or the springs between belts and slides, experiments were done with only the motor. For this purpose a belt was detached from the motor shaft. Then the controlled system only consists of the motor. The applied forces of experiments with:

$$\omega_{ox} = 10{\times}2\pi \text{ [rad/s]} \hat{=} 10 \text{ [Hz]}, \beta_x = 1$$

$$\omega_{ox} = 15{\times}2\pi \text{ [rad/s]} \hat{=} 15 \text{ [Hz]}, \beta_x = 1 \qquad (5.9)$$

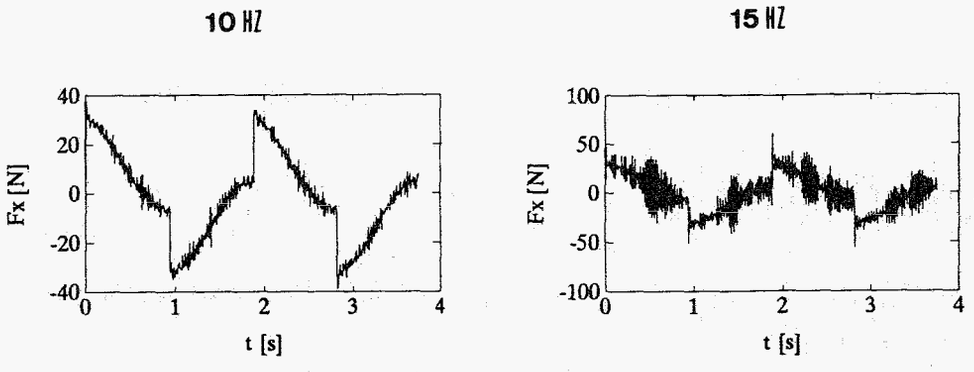

Figure 5.2: Applied forces to motor

are shown in figure 5.2. The same kind of vibrations occur. At 15 [Hz] the input force shows the same chattering as the experiment with the total system at 10 [Hz]. Apparently the chattering is influenced by the dynamics of the XY–table, for the chattering starts at different eigenfrequencies and with an other amplitude. But because chattering was also shown in the experiments with the detached belt, the main cause can only be one or more of the following model errors:

- o Dynamics of motor and/or amplifier
- o Estimation errors of Kalman observer
- o Sampling frequency

The estimation errors of the Kalman observer can be determined after the experiment. The estimation errors of the position can be neglected. The actual speed is determined using a central difference method:

$$\dot{x}(t) = \frac{x(t+T_s) - x(t-T_s)}{2\ T_s}$$

T_s : Sampling time (5.10)

Now the estimation errors are written as:

$$v(t) = \dot{x}(t) - \dot{\hat{x}}(t)$$

$\dot{\hat{x}}(t)$: Estimated speed (5.11)

A part of the calculated input force is the result of these estimation errors. The standard deviation of the estimation errors in the experiment with the total system at 5 [Hz] is:

$$S_v = 4\ [mm/s] \tag{5.12}$$

The standard deviation of the part of the calculated input force due to estimation errors is then:

$$S_f = K_d\, S_v = 2\beta\omega_{ox} P_1\, S_v$$

$$S_f = 2{\times}1{\times}5{\times}2\pi{\times}46.5{\times}4\ [mN] \hat{=} 12\ [N] \tag{5.13}$$

This explains the little vibrations of the input force at 5 [Hz] in figure 5.1. At 10 [Hz] the part of the force due to estimation errors would be expected to be twice as large because of a twice as large ω_{ox}. But the deviation of the estimation errors has become larger too:

$$S_v = 12\ [mm/s] \tag{5.14}$$

This causes a standard deviation in the input force at 10 [Hz]:

$$S_f = 2{\times}1{\times}10{\times}2\pi{\times}46.5{\times}12\ [mN] \hat{=} 70\ [N] \tag{5.15}$$

This explains the chattering response of the XY–table at 10 [Hz]. But why does the standard deviation of the estimation errors become larger at higher eigenfrequencies. Because the same effects occur, when only the motor is controlled, the only possible reasons can be:

- o Dynamics of motor and/or amplifier
- o Sampling frequency

Experiments with the XY–table were done to look at the influence of the sampling frequency on the estimation errors. The desired trajectory was:

$$x_d = M - R\cos(2\pi ft),\ y_d = 800$$
$$M = 800\ [mm],\ R = 150\ [mm],\ f = \tfrac{1}{2}\ [Hz]$$
$$0 \leq t \leq 2\ [s] \qquad (5.16)$$

The sampling frequencies were chosen to be 125 [Hz] and 250 [Hz]. The sampling frequency of 250 [Hz] had been made possible by letting the computer only calculate the PD feedback in X–direction.

With a sampling frequency of 125 [Hz] the chattering response begins above an eigenfrequency of 5 [Hz]. The standard deviation of the estimation errors at 10 [Hz] is almost ten times larger than at 5 [Hz].

With a sampling frequency of 250 [Hz] the chattering response begins above an eigenfrequency of 20 [Hz]. At 5 [Hz] the standard deviation of the estimation errors is about the same as with a sampling frequency of 125 [Hz]. But now even at 20 [Hz] the standard deviation has not changed appreciably. To prove that the sampling frequency is the cause of the increased standard deviation of (5.14), the estimation errors of the Kalman filters with 125 [Hz] and 250 [Hz] should be compared, when the same input signal is applied. Dynamics of motor and/or amplifier can still cause chattering, when the effects of the sampling frequency are not shown to be qualitatively equal to the total effects. However there was no time left to do these experiments during this study.

The chattering response is caused by the estimation errors of the Kalman observer. Probably the sampling frequency of 125 [Hz] makes the speed estimation worse above an eigenfrequency of 5 [Hz], but to prove this some experiments should be done. Because the implementation of the adaptive controller in X– and Y–direction needs a sampling time of about 8 [ms], the sampling frequency cannot be larger than 125 [Hz]. This means that in X–direction a chattering response is caused at an eigenfrequency of about 5 [Hz], probably by:

- o Estimation errors of Kalman observer
- o Influence sampling frequency on Kalman observer

In Y–direction a chattering response is caused by the same reasons at about the same eigenfrequency.

5.5 Rigid system experiments

Experiments with the rigid system (rigid bar) were done to compare the PD and adaptive controller with a sampling frequency of 125 [Hz]. The gain matrices of the PD controller were chosen according to equations (5.6) with:

$$\omega_{ox} = \omega_{oy} = 4{\times}2\pi \text{ [rad/s]}$$
$$\beta_x = \beta_y = 0.7 \qquad (5.17)$$

This was the largest possible eigenfrequency without appreciable influence of the estimation errors of the Kalman observer on the calculated input force. Now undesirable chattering response was totally avoided. To determine the largest possible gain matrices of the adaptive controller, which did not cause chattering at all, the parameters were chosen as hundred percent parameters with adaptation off. This resulted in the same gain matrices as for the PD controller. The desired path was:

$$x_d = y_d = M - R\cos(2\pi ft)$$
$$M = 800 \text{ [mm]},\ R = 150 \text{ [mm]},\ f = \frac{1}{2} \text{ [Hz]}$$
First control cycle $0 \leq t \leq 4$ [s]

Second control cycle $4 \leq t \leq 8$ [s]

Third control cycle $8 \leq t \leq 12$ [s] (5.18)

Of course the results of the PD controller stay the same for each control cycle (except the effects of initial conditions), because the desired path stays the same. But the results of the adaptive controller are different, because each control cycle starts with the last parameter values of the previous control cycle. In appendix F the design of the adaptive controller is given. The adaptation values are determined such that the adaptation process is slower than the control bandwidth. Then the adaptive controller with adaptation on will not cause chattering, when the adaptive controller with adaptation off does not cause chattering. The experiments were:

1: PD controller without friction compensation

2: adaptive controller starting from zero estimates:
results of first control cycle

3: adaptive controller starting from zero estimates:
results of third control cycle

4: PD controller with 75 % friction compensation:

5: adaptive controller starting from 75 % estimates:
results of first control cycle

6: adaptive controller starting from 75 % estimates:
results of third control cycle

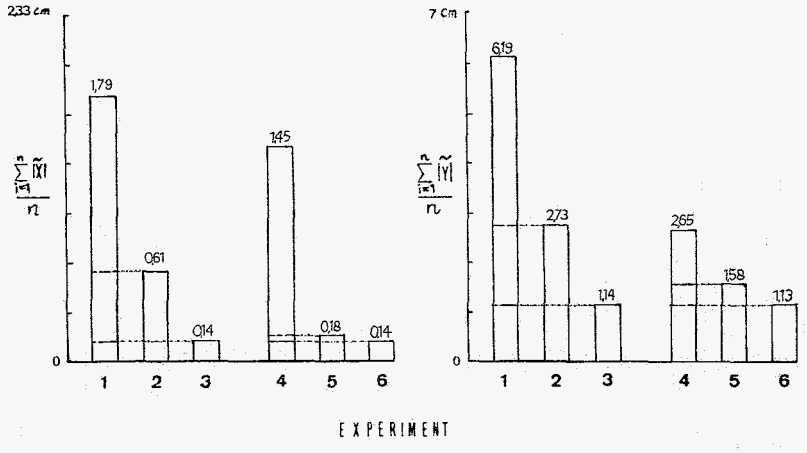

Figure 5.3: Mean absolute tracking errors of motor position

The mean absolute tracking errors of all experiments are shown in figure 5.3. The performance of the adaptive controller is much better than of the PD controller. At the third control cycle the results of the adaptive controller starting with 0 % and 75 % parameter estimates are the same. For the third control cycle it does not matter, what the initial parameter values were. The adaptive controller is able to estimate the same parameters after two control cycles, no matter what the initial values were. In figure 5.4 the parameter estimates of the adaptive controller starting from zero estimates are shown during the first and third control cycle. During the third control cycle the parameters do not really change, but fluctuate around a mean value. The parameters can be expressed with a mean value plus minus a percentage, which represents the standard deviation of the fluctuations:

Estimates:	Model:	
$\hat{P}_1 = 47.4$ [kg] ± 0.9 %	$P_1 = 46.5$ [kg]	
$\hat{P}_2 = 4.10$ [kg] ± 9.0 %	$P_2 = 4.30$ [kg]	
$\hat{P}_3 = 42.2$ [N] ± 1.1 %	$P_3 = 50.0$ [N]	
$\hat{P}_4 = 17.7$ [N] ± 1.5 %	$P_4 = 15.0$ [N]	(5.19)

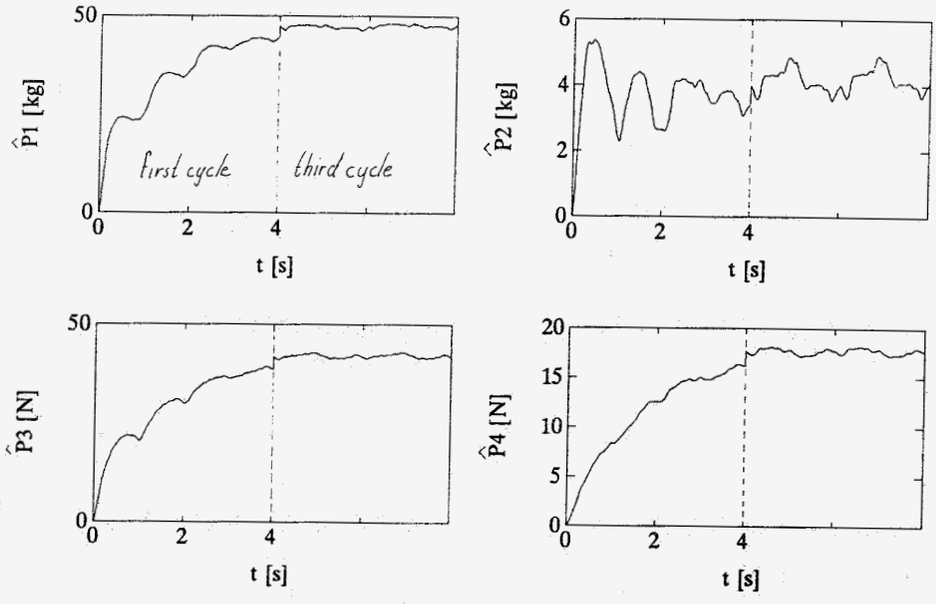

Figure 5.4: Parameter estimates

The estimated parameters correspond better to the actual system parameters than the model parameters, which were used for the design of controllers and Kalman observer. The model parameters were only rough indications used, because there was no better information available. The fluctuations of the second parameter (the mass in Y–direction) are larger than the other fluctuations. The plots of the tracking errors of experiment 1 (PD) and 3 (adaptive) are shown in figure 5.5.

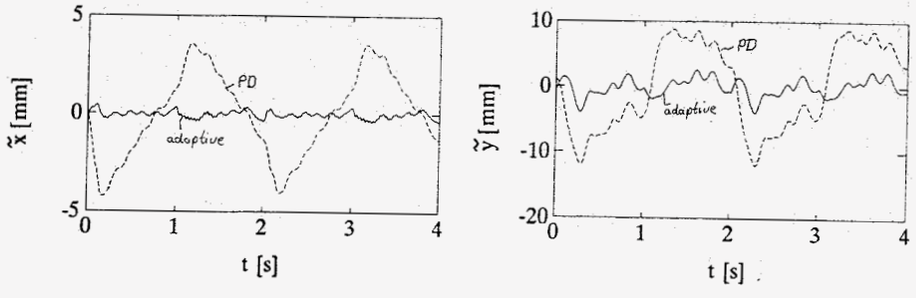

Figure 5.5: Tracking errors of motor position

In X–direction the tracking errors of the adaptive controller are much smaller in comparison with the PD controller. The remaining tracking errors can mainly be attributed to unmodelled dynamics:

- o The little springs between belts and slides
- o Backlash in one of the bearings
- o Contact between belts and sides of belt wheels
- o Dynamics of motor and amplifier
- o Harmonic friction term

Especially the influence of the harmonic friction is shown very clearly. Each revolution of a bearing shaft corresponds to one 'vibration' in the plot of the tracking errors.

In Y–direction the tracking errors of the adaptive controller are smaller compared with the PD controller, but the difference is not as big as in X–direction. The remaining tracking errors can mainly be attributed to:

- o The little springs between belt and slide
- o Contact between belt and sides of belt wheels
- o Dynamics of motor and amplifier
- o Harmonic friction term

Again the harmonic friction term is shown very clearly in figure 5.5. The influence of the harmonic friction has much more influence on the tracking errors than in X–direction. The harmonic friction term in Y–direction is much larger with regard to the input force than in X–direction. Because of this the modelling error due to the harmonic friction is relatively larger in Y–direction than in X–direction. Therefore the adaptive controller has the best results in X–direction, although the results of the adaptive controller in Y–direction are also much better than the the results of the PD controller. The relatively larger model errors are probably the reason that the mass parameter in Y–direction shows large fluctuations.

The adaptive controller achieves much better results than the PD controller. The parameter estimates converge very well to constant values within some fluctuations. The remaining tracking errors of the adaptive controller are caused by unmodelled dynamics. How large the influence of the different modelling errors is on the tracking errors, could be determined with simple experiments. For example the influence of the little springs could be investigated by doing the same experiments with a stiff construction between belts and slides.

The influence of the harmonic friction due to bad bearings could be examined by replacing these bearings. Or, what would even be more interesting, by expanding the model used for the adaptive controller design with harmonic friction.

5.6 Flexible system experiments

The previous experiments were done with a rigid bar. The rigid bar was replaced by a flexible one to add some extra unmodelled dynamics. Nothing else was changed. The sampling frequency, the desired trajectory, the Kalman observer and the model used for controller design stayed the same. Now the eigenfrequency of 4 [Hz] in X–direction causes undesirable chattering. To avoid this chattering the maximum possible eigenfrequencies in X–direction are:

PD controller:

$$\omega_{ox} = 3.5 \times 2\pi \text{ [rad/s]}$$
$$\beta_x = 0.7 \qquad (5.20)$$

Adaptive controller:

$$\omega_{ox} = 2.5 \times 2\pi \text{ [rad/s]}$$
$$\beta_x = 0.7 \qquad (5.21)$$

Again the chattering at higher eigenfrequencies will probably have something to do with the Kalman observer and the sampling frequency. But the direct cause must be the flexible bar, for this is the only thing that has been changed. A remarkable fact is that the eigenfrequency and thus the gain matrices of the adaptive controller must be smaller than the PD controller. The adaptive controller is less robust to the unmodelled dynamics than the PD controller. The adaptive controller does not have to have essentially the same level of robustness to unmodelled dynamics as was suggested by Slotine and Li (1987).

The adaptation values in the experiments with a rigid bar, which were determined in X–direction for an eigenfrequency of 4 [Hz], were still used in the experiments with a flexible bar with eigenfrequency of 2.5 [Hz] in X–direction. The adaptation values were chosen so small that the adaptation process was much slower than the control bandwidth. Then, with the same adaptation values, the adaptation process will still be smaller than the control bandwidth at 2.5 [Hz].

The experiments were again:

1: PD controller without friction compensation

2: adaptive controller starting from zero estimates:
results of first control cycle

3: adaptive controller starting from zero estimates:
results of third control cycle

4: PD controller with 75 % friction compensation:

5: adaptive controller starting from 75 % estimates:
results of first control cycle

6: adaptive controller starting from 75 % estimates:
results of third control cycle

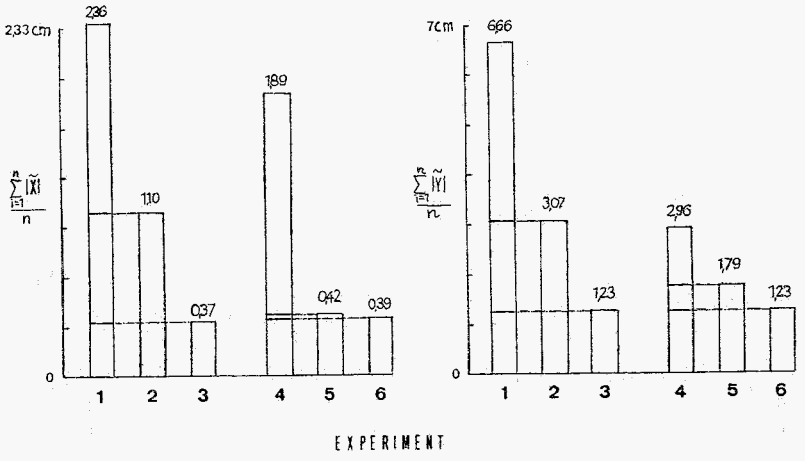

Figure 5.6: Mean absolute tracking errors of motor position

The mean absolute tracking errors are shown in figure 5.6. The adaptive controller is less robust to unmodelled dynamics, through which the gain matrices must be smaller, but achieves much better tracking accuracy than the PD controller. The estimated parameters plus minus a standard deviation during the third control cycle starting from zero estimates are:

Estimates:	Model:	
$\hat{P}_1 = 48.0$ [kg] ± 2.2 %	$P_1 = 46.5$ [kg]	
$\hat{P}_2 = 4.23$ [kg] ± 8.3 %	$P_2 = 4.30$ [kg]	
$\hat{P}_3 = 43.7$ [N] ± 2.5 %	$P_3 = 50.0$ [N]	
$\hat{P}_4 = 19.1$ [N] ± 1.8 %	$P_4 = 15.0$ [N]	(5.22)

The plots of the tracking errors of experiment 1 (PD) and 3 (adaptive) are shown in figure 5.7. The remaining tracking errors of the adaptive controller can be attributed to the same sources as with the rigid bar. The only added source is the error due to the flexible bar. Of course the flexible bar especially influences the tracking errors in X–direction.

The adaptive controller shows very good results. In paragraph 5.4 the influence of the Kalman observer was discussed. The Kalman observer was designed with the model parameters of equations (5.2). The Kalman observer could be improved by using the estimated parameters of equations (5.22), by expanding the Kalman observer model with harmonic friction, and by using a stiff construction between belts and slides instead of the flexible springs. This would decrease the process noise.

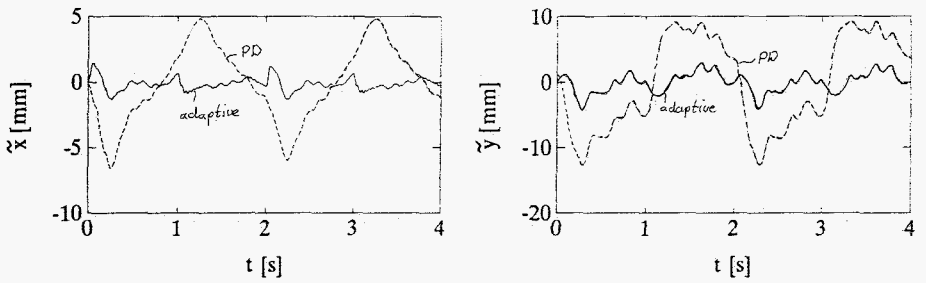

Figure 5.7: Tracking errors of motor position

5.7 Conclusions

Experiments with the flexible XY–table show that the adaptive controller is less robust to unmodelled dynamics, but achieves much better tracking accuracy than the PD controller. The parameter estimates converge to constant values plus minus some small fluctuations. These values are the same no matter what the initial estimates are. The fluctuations are caused by unmodelled dynamics and measurement noise.

When the parameter estimates have reached their "constant" values, the remaining tracking errors are caused by unmodelled dynamics and measurement noise. A structural better model results in smaller tracking errors. The adaptive controller is able to estimate the parameters well. Especially when manipulators have to handle large unknown loads, or parameters are unknown for other reasons, the adaptive controller is recommended. For, despite all non parametric error sources of the flexible XY–table, the adaptive controller achieves much better tracking accuracy than the PD controller.

Chattering response of the XY–table is caused by the errors in the speed estimation of the Kalman observer and probably by the influence of the sampling frequency on the Kalman observer. The Kalman observer could be improved by using the estimated parameter values of the adaptive controller, by expanding the Kalman observer model with harmonic friction, and by using a stiff construction between belts and slides. The sampling frequency could be increased by using faster computers.

A large part of the tracking errors is caused by the harmonic friction due to bad bearings. It would be interesting to expand the model, used for the adaptive controller design, with the harmonic friction.

CHAPTER 6: CONCLUSIONS AND RECOMMENDATIONS

In this chapter the most important conclusions are summarized and recommendations are given for further experiments and research:

- The parameter estimates do not converge to their exact physical values because of unmodelled dynamics and measurement noise. Due to these unmodelled dynamics and measurement noise the parameter estimates do not converge to constant values, but stay fluctuating a little. For smooth parameter estimates the adaptation process is chosen slower than the control bandwidth. When the adaptation process is chosen as fast as the control bandwidth, the adaptive controller could for example estimate a constant mass with a time dependent friction. Then the friction parameter is not estimated smoothly. And the fluctuations due to unmodelled dynamics will be larger. An extra remark: When there are no unmodelled dynamics or measurement noise, convergence of the trajectory tracking is guaranteed. But to guarantee exact parameter convergence, the desired trajectory must be sufficiently rich so that only the true set of parameters can yield exact tracking (Slotine and Li, 1987).

- The adaptive controller, applied to the flexible XY–table, is less robust with respect to unmodelled dynamics and/or measurement noise than the PD controller. But because the parameters are estimated very well, the adaptive controller achieves better tracking accuracy than the PD controller. The adaptive controller is recommended, especially when parameters are unknown. For example when mechanical manipulators have to handle large unknown loads.

- When the gain matrices of the PD feedback are chosen too large, a chattering response of the XY–table will arise. This chattering response is caused by the errors of the speed estimation. This speed is estimated by a Kalman observer. The sampling frequency has great influence on the estimation errors. The Kalman observer could easily be improved by using the estimated parameters from the adaptive controller, by expanding the Kalman observer with harmonic friction, by using a stiff construction between belts and slides, and by increasing the sampling frequency. The sampling frequency can be increased by replacing the PC by a faster compatible model.

- The estimated parameters "converge" always to the same values (within some fluctuations), no matter what the initial values are. The converged parameters are not entirely constant because of little fluctuations due to unmodelled dynamics. These unmodelled dynamics are the reason that the tracking errors are not zero, when the parameters have converged. Besides the unmodelled torsion spring there are other sources of the remaining tracking errors: flexible springs between belts and slides, backlash in one of the bearings, harmonic friction due to bad bearings, dynamics of motors and amplifier, contact between belts and the sides of belt wheels.

- It would be useful to investigate the influence of the different model errors on the remaining tracking errors of the adaptive controller. The flexible springs between belts and slides could be replaced by a stiff construction. The difference between the remaining tracking errors with and without these springs is the influence of these springs. The influence of the harmonic friction, which is clearly present, could be investigated by replacing the bad bearings. Or even more interesting would be to add harmonic friction to the adaptive controller model and, doing so, compensate this friction.

- The optical measurement system, which measures the end–effector position, could not be used during this study. Only motor rotations were measured. When the end–effector position is available, it would be possible to tune the XY–table by finding the optimal weighing factors between motor and end–effector feedback. In the simulations it has been shown that only end–effector feedback could cause instability problems. Again the results of PD and adaptive controller could be compared.

- The software, which controls the XY–table, is in Turbo Pascal. After each experiment it is possible to watch plots of the results inside the Turbo Pascal program. But a new experiment deletes the data of the previous experiment. It is not possible to compare plots of two experiments inside the Turbo Pascal program. The program is expanded with an option to save results in a Matlab–file. But then it is only possible to compare different experiments outside the Turbo Pascal program. It would be much easier, if the program was written in Matlab. Only the real time part, the control algorithm, should be in a compiled language. Then several experiments could be compared, which could save a lot of time.

- Further research should be done into robust controllers, which are proposed in literature, by implementation at the XY–table. The performance of these controllers can be compared with the PD and the adaptive controller of Slotine and Li.

APPENDIX A: ADAPTIVE CONTROLLER DESIGN FOR RT–ROBOT

In this appendix the adaptive controller is designed according to chapter 2 for the RT–robot of chapter 3.

System:

$$H(q)\ddot{q} + C(q,\dot{q})\dot{q} + g(q) = \tau \tag{2.1}$$

Control law:

$$\tau = \hat{H}(q)\ddot{q}_r + \hat{C}(q,\dot{q})\dot{q}_r + \hat{g}(q) - K_d s \tag{2.2}$$

$$\tau = Y(q,\dot{q},\dot{q}_r,\ddot{q}_r)\hat{a} - K_d s \tag{2.3}$$

Adaptation law:

$$\dot{\hat{a}} = -\Gamma^{-1}Y^T(q,\dot{q},\dot{q}_r,\ddot{q}_r)s \tag{2.4}$$

This yields for RT–robot with dynamic equations (3.1):

$$H = \begin{bmatrix} m+m_1 & 0 \\ 0 & I+\frac{1}{3}ml^2-mlr+(m+m_1)r^2 \end{bmatrix}$$

$$C = \begin{bmatrix} 0 & -\{(m+m_1)r-\frac{1}{2}ml\}\dot{\varphi} \\ \{(m+m_1)r-\frac{1}{2}ml\}\dot{\varphi} & \{(m+m_1)r-\frac{1}{2}ml\}\dot{r} \end{bmatrix}$$

$$g = \begin{bmatrix} 0 \\ 0 \end{bmatrix}$$

$$\tau = \begin{bmatrix} F \\ M \end{bmatrix} \quad q = \begin{bmatrix} r \\ \varphi \end{bmatrix} \quad a^T = [P_1\ P_2\ P_3]$$

$$Y = \begin{bmatrix} \ddot{r}_r - r\dot{\varphi}\dot{\varphi}_r & \dot{\varphi}\dot{\varphi}_r & 0 \\ r^2\ddot{\varphi}_r + r\dot{\varphi}\dot{r}_r + r\dot{r}\dot{\varphi}_r & -2r\ddot{\varphi}_r - \dot{\varphi}\dot{r}_r - \dot{r}\dot{\varphi}_r & \ddot{\varphi}r \end{bmatrix} \tag{A.1}$$

or with friction:

$$\tau = \begin{bmatrix} F \\ M \end{bmatrix} \quad q = \begin{bmatrix} r \\ \varphi \end{bmatrix} \quad a^T = [P_1\ P_2\ P_3\ P_4\ P_5]$$

$$Y = \begin{bmatrix} \ddot{r}_r - r\dot{\varphi}\dot{\varphi}_r & \dot{\varphi}\dot{\varphi}_r & 0 & \text{sign}(\dot{r}) & \dot{r} \\ r^2\ddot{\varphi}_r + r\dot{\varphi}\dot{r}_r + r\dot{r}\dot{\varphi}_r & -2r\ddot{\varphi}_r - \dot{\varphi}\dot{r}_r - \dot{r}\dot{\varphi}_r & \ddot{\varphi}r & 0 & 0 \end{bmatrix} \tag{A.2}$$

Except for the choices of K_d, K_p $(= K_d\Lambda)$ and Γ^{-1} the adaptive controller is totally defined.

APPENDIX B: ADAPTATION VALUES FOR RT–ROBOT

In this appendix the adaptation values are determined for the RT–robot with friction and unmodelled dynamics. The adaptation values have to be chosen small enough so that the bandwidth of the controlled system stays smaller than the bandwidth of the unmodelled dynamics. The unmodelled dynamics (see equations 3.12) have an eigenfrequency of 25 [rad/s]. The poles of the controlled system are determined by linearization of the controlled system at different points of time (different points on the desired trajectory). A representative point of time is:

$$t = 0.27 \text{ [s]}.$$

In paragraph 3.3 the PD controller is designed to create eigenfrequencies and damping factors (in r– and φ–direction):

$$\begin{aligned} \omega_0 &= 10 \text{ [rad/s]} \\ \beta &= 1 \text{ [–]} \end{aligned} \qquad (3.2)$$

With this eigenfrequency the bandwidth of the controlled system is smaller than the bandwidth of the unmodelled dynamics. The poles of the controlled linearized system at t = 0.27 [s] are:

$$\text{poles with PD controller} \begin{bmatrix} -10 \\ -10 \\ -10 \\ -10 \end{bmatrix} \begin{matrix} \} \\ \\ \\ \} \end{matrix} \begin{matrix} \text{r–direction} \\ \\ \\ \varphi\text{–direction} \end{matrix}$$

The adaptive controller with *hundred percent parameters* and adaptation off results in the following poles of the controlled system:

$$\text{poles with adaptation off} \begin{bmatrix} -20 \\ -5 \\ -20 \\ -5 \end{bmatrix} \begin{matrix} \} \\ \\ \\ \} \end{matrix} \begin{matrix} \text{r–direction} \\ \\ \\ \varphi\text{–direction} \end{matrix}$$

These poles are equivalent with:

$$\begin{aligned} \omega_0 &= 10 \text{ [rad/s]} \\ \beta &= 1.25 \text{ [–]} \end{aligned}$$

The eigenfrequency has stayed exactly the same as in (3.2). The hundred percent parameters only cause larger damping, by which two poles have become smaller and two poles have become larger. Although two poles have become 20 [rad/s], they will not cause instability. The amplitude response starts decreasing at frequencies above 5 [rad/s]. So the amplitude of input signals with frequency 20 [rad/s] will decrease a lot. When the

eigenfrequency stays the same and the damping factor increases, the controlled system becomes slower. The adaptive controller with hundred percent parameters and adaptation off will not cause instabilities.

Now the adaptation values have to be chosen small enough to avoid instabilities. When

$$\Gamma^{-1} = \begin{bmatrix} 3 & 0 & 0 & 0 & 0 \\ 0 & 3 & 0 & 0 & 0 \\ 0 & 0 & 3 & 0 & 0 \\ 0 & 0 & 0 & 500 & 0 \\ 0 & 0 & 0 & 0 & 500 \end{bmatrix}$$

the poles of the linearized controlled system are:

$$\text{poles with adaptation on} \begin{bmatrix} -16.4 \\ -14.1 \\ -3.7 \\ -5.5+0.6j \\ -5.5-0.6j \\ -5.0 \\ 0.0 \\ 0.0 \\ 0.0 \end{bmatrix}$$

The extra poles are from the adaptation law. The sequence of the above poles is arbitrary. The bandwidth with these poles will not have increased significantly in proportion to the bandwidth with adaptation off. With the chosen Γ^{-1} no instabilities will occur. But it is clear that the influence of the adaptation on the poles is not small. For smooth parameter estimates, the adaptation process should be much slower than the control bandwidth. Now it is possible that, for example, a constant mass parameter is partly estimated as a time dependent friction. In that case the friction parameter will not converge smoothly.

APPENDIX C: DERIVATION OF XY–TABLE MODEL

In this appendix the equations of motion of the simulated system from figure 4.2 in chapter 4 are given with the values used for all parameters. For the sake of convenience figure 4.2 is shown again.

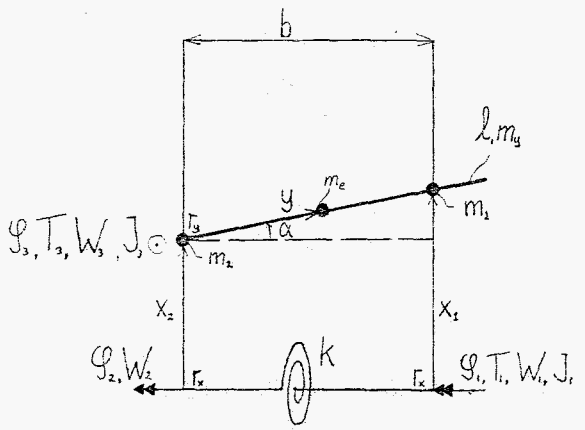

Figure 4.2: Simulated system

The used symbols of figure 4.2 are:

φ_1	angular displacement of belt wheel 1
φ_2	angular displacement of belt wheel 2
φ_3	angular displacement of belt wheel 3
x_1	position of x–slide 1 on slideway 1
x_2	position of x–slide 2 on slideway 2
y	position of the end–effector on the y–slideway
b	distance between slideway 1 and 2
l	length of the y–slideway
r_x	radius of the belt wheels 1 and 2
r_y	radius of belt wheel 3
m_1	mass of x–slide 1
m_2	mass of x–slide 2
m_e	mass of the end–effector
m_y	mass of the y–slideway including the y–motor
J_1	moment of inertia associated with φ_1
J_2	J_2 (moment of inertia associated with φ_2) is assumed to be zero

J_3	moment of inertia associated with φ_3
W_1	friction torque associated with φ_1
W_2	friction torque associated with φ_2
W_3	friction torque associated with φ_3
T_1	motor torque on belt wheel 1
T_3	motor torque on belt wheel 3
k	spring constant

$x_1 = \varphi_1 r_x$

$x_2 = \varphi_2 r_x$

$y = \varphi_3 r_y$

$\alpha = \arctan(\frac{x_1 - x_2}{b})$

The values used in the simulations are:

$b = 1$ [m]	$l = 1$ [m]
$r_x = 0.01$ [m]	$r_y = 0.01$ [m]
$m_1 = 3.8$ [kg]	$m_2 = 3.8$ [kg]
$m_e = 2.3$ [kg]	$m_y = 8.5$ [kg]
$J_1 = 5 \times 10^{-4}$ [kgm^2]	$J_3 = 5 \times 10^{-5}$ [kgm^2]
$W_1 = 0.2$ [Nm]	$W_2 = 0.2$ [Nm]
$W_3 = 0.02$ [Nm]	$k = 0.2$ [Nm/rad]

Remark: These parameters do not correspond to the parameters of the actual XY–table

All masses are considered point masses. The angle α is assumed to be small:

$$\alpha \simeq \frac{x1 - x2}{b} \; ; \; \cos\alpha \simeq 1 \; ; \; \sin\alpha \simeq \alpha$$

The equations of motion of the simulated system, derived with the help of the method of Lagrange and the software package MAPLE, are

$$M(q)\ddot{q} + h(q,\dot{q}) = f \qquad \text{(C.1)}$$

with

$$q^T = [\varphi_1\ \varphi_2\ \varphi_3]$$
$$M_{11} = J_1 + [m_1 + \tfrac{1}{3}m_y(\tfrac{l}{b})^2 + m_e(\tfrac{\varphi_3 r_y}{b})^2]r_x^2$$
$$M_{12} = M_{21} = [\tfrac{1}{2}m_y(\tfrac{l}{b}) - \tfrac{1}{3}m_y(\tfrac{l}{b})^2 + m_e(\tfrac{\varphi_3 r_y}{b}) - m_e(\tfrac{\varphi_3 r_y}{b})^2]r_x^2$$
$$M_{13} = M_{31} = 0$$
$$M_{22} = [m_2 + m_y - m_y(\tfrac{l}{b}) + \tfrac{1}{3}m_y(\tfrac{l}{b})^2 + m_e - 2m_e(\tfrac{\varphi_3 r_y}{b}) + m_e(\tfrac{\varphi_3 r_y}{b})^2]r_x^2$$
$$M_{23} = M_{32} = [m_e\frac{(\varphi_1 - \varphi_2)r_y}{b}]r_x^2$$
$$M_{33} = J_3 + m_e r_y^2$$
$$h_1 = 2m_e(\varphi_3 r_y)\frac{r_y r_x^2}{b^2}(\dot{\varphi}_1 - \dot{\varphi}_2)\dot{\varphi}_3 + k(\varphi_1 - \varphi_2)$$
$$h_2 = 2m_e(b - \varphi_3 r_y)\frac{r_y r_x^2}{b^2}(\dot{\varphi}_1 - \dot{\varphi}_2)\dot{\varphi}_3 - k(\varphi_1 - \varphi_2)$$
$$h_3 = -m_e(\varphi_3 r_y)\frac{r_y r_x^2}{b^2}(\dot{\varphi}_1 - \dot{\varphi}_2)^2$$
$$f_1 = T_1 - W_1 sign(\dot{\varphi}_1)$$
$$f_2 = -W_2 sign(\dot{\varphi}_2)$$
$$f_3 = T_3 - W_3 sign(\dot{\varphi}_3)$$

Equations (C.1) are used for the simulated system. The model used for controller design is simplified by assuming that there is no torsion spring. Then the angles φ_1 and φ_2 are exactly the same. If the torsion spring is unmodelled, equations (C.1) can be replaced by:

$$M(q)\ddot{q} + w(\dot{q}) = \tau \qquad \text{(C.2)}$$

with

$$q^T = [\varphi_1\ \varphi_3]$$
$$M_{11} = J_1 + [m_1 + m_2 + m_e + m_y]r_x^2$$
$$M_{12} = M_{21} = 0$$
$$M_{22} = J_3 + m_e r_y^2$$
$$w_1 = (W_1 + W_2)sign(\dot{\varphi}_1)$$
$$w_2 = W_3 sign(\dot{\varphi}_3)$$
$$\tau_1 = T_1$$
$$\tau_2 = T_3$$

The values of the parameters are:

$P_1 = M_{11} = 2.34 \times 10^{-3}$ [kgm^2]
$P_2 = M_{22} = 2.80 \times 10^{-4}$ [kgm^2]
$P_3 = W_1 + W_2 = 0.40$ [Nm]
$P_4 = W_3 = 0.02$ [Nm]

APPENDIX D: ADAPTIVE CONTROLLER DESIGN FOR XY–TABLE

In this appendix the adaptive controller is designed according to chapter 2 for the simulated XY–table of chapter 4.

System:

$$H(q)\ddot{q} + w(\dot{q}) = \tau$$

Control law:

$$\tau = \hat{H}(q)\ddot{q}_r + \hat{w}(q) - K_d s$$

$$\tau = Y(q,\dot{q},\dot{q}_r,\ddot{q}_r)\hat{a} - K_d s \qquad (2.3)$$

Adaptation law:

$$\dot{\hat{a}} = -\Gamma^{-1} Y^T(q,\dot{q},\dot{q}_r,\ddot{q}_r)s \qquad (2.4)$$

This yields for XY–table with dynamic equations (4.1):

$$H = \begin{bmatrix} P_1 & 0 \\ 0 & P_2 \end{bmatrix} \quad w = \begin{bmatrix} P_3 \mathrm{sign}(\dot{\varphi}_1) \\ P_4 \mathrm{sign}(\dot{\varphi}_3) \end{bmatrix}$$

$$\tau = \begin{bmatrix} T_1 \\ T_3 \end{bmatrix} \quad q = \begin{bmatrix} \varphi_1 \\ \varphi_3 \end{bmatrix} \quad a^T = [P_1\ P_2\ P_3\ P_4]$$

$$Y = \begin{bmatrix} \ddot{\varphi}_{1r} & 0 & \mathrm{sign}(\dot{\varphi}_1) & \\ 0 & \ddot{\varphi}_{3r} & 0 & \mathrm{sign}(\dot{\varphi}_3) \end{bmatrix} \qquad (D.1)$$

Now the adaptation values are determined for the XY–table. For a good comparison the bandwidth of the system with adaptive controller is not allowed to be larger than the bandwidth of the system with PD controller. The poles of the controlled system are determined by linearization of the controlled system at different points of time (different points of desired trajectory). The poles are determined of the system with torsion spring. A representative point of time is:

$$t = 0.125 \text{ [s]}.$$

In paragraph 4.3 the PD controller is designed to create eigenfrequencies of 10 [rad/s] for the simplified model of equations (4.3). The poles of the controlled linearized system with torsion spring at t = 0.125 [s] are:

$$\text{poles with PD controller} \begin{bmatrix} -3.3 + 21.2j \\ -3.3 - 21.2j \\ -13.5 \\ -9.0 \\ -10.0 \\ -10.0 \end{bmatrix}$$

The simplified model, a second order system with degrees of freedom φ_1 and φ_3, would have shown four poles with value -10. But the poles of the simulated system, a third order system with degrees of freedom φ_1, φ_2 and φ_3, are influenced by the torsion spring. In paragraph 4.6 discretization effects are discussed. The mentioned frequency of 3.4 [Hz] can be derived with:

$$\text{Maximum response frequency} \approx \frac{\sqrt{3.3^2 + 21.1^2}}{2\pi} = 3.4 \text{ [Hz]}$$

The adaptive controller with *hundred percent parameters* and adaptation off results in the following poles of the controlled system:

$$\text{poles with adaptation off} \begin{bmatrix} -2.8 + 20.7j \\ -2.8 - 20.7j \\ -25.6 \\ -5.0 \\ -5.0 \\ -20.0 \end{bmatrix}$$

The hundred percent parameters cause larger damping, through which two poles have become much smaller and two poles have become much larger. Although two poles have become 20 [rad/s] and 25.6 [rad/s], they will not cause instability. The amplitude response starts decreasing at frequencies above 5 [rad/s]. So the amplitude of input signals with frequency 20 [rad/s] will decrease a lot. The adaptive controller with hundred percent parameters and adaptation off will not cause instabilities.

Now the adaptation values have to be chosen small enough. When

$$\Gamma^{-1} = \begin{bmatrix} 2.5\times10^{-7} & 0 & 0 & 0 \\ 0 & 2.5\times10^{-8} & 0 & 0 \\ 0 & 0 & 1.0\times10^{-1} & 0 \\ 0 & 0 & 0 & 1.0\times10^{-2} \end{bmatrix}$$

the poles of the linearized controlled system are:

$$\text{poles with adaptation on} \begin{bmatrix} -3.4 + 20.4j \\ -3.4 - 20.4j \\ -17.1 \\ -14.7 \\ -7.0 \\ -6,0 \\ -4.9 + 0.3j \\ -4.9 - 0.3j \\ 0,0 \\ 0,0 \end{bmatrix}$$

The extra poles are from the adaptation law. The sequence of the above poles is arbitrary. The bandwidth with these poles will not have increased in proportion to the bandwidth with adaptation off. But it is clear that the influence of the adaptation on the poles is not small. For smooth parameter estimates the adaptation process should be much slower than the control bandwidth. This fact will be reckoned with in the practical experiments with the XY–table.

APPENDIX E: DESIGN OF KALMAN OBSERVER

A Kalman observer is designed to estimate the position and speed one sample ahead. Then there are no time delays. The simplified model of the actual XY–table is:

$$P_1\ddot{x} = F_1 - P_3\text{sign}(\dot{x})$$
$$P_2\ddot{y} = F_3 - P_4\text{sign}(\dot{y}) \qquad (5.1)$$

First the Kalman observer will be designed in x–direction. The design will be based on a discrete time model to make no discretization errors. Because the Kalman observer must be able to work with different sampling frequencies, the discrete time model is derived as function of the sampling time. The second order differential equation in x–direction can be represented as a set of two first order differential equations. First a state vector, the control input and the output are defined:

$$\text{State: } x(t) = \begin{bmatrix} x(t) \\ \dot{x}(t) \end{bmatrix}$$
$$\text{Input: } u(t) = F_1$$
$$\text{Output: } y(t) = x(t)$$

Because the model is a simplification of the actual system, there will be process noise w(t). This process noise is modelled as noise on input u(t). Whether this is correct, will be verified later on. Then the first order differential equations are:

$$\dot{x}_1(t) = \dot{x}(t) = x_2(t)$$
$$\dot{x}_2(t) = \ddot{x}(t) = \frac{1}{P_1}[u(t) + w(t) - P_2\text{sign}(\dot{x}(t))]$$

With sampling time T_s and measurement noise v(t) the discrete time model can be written as:

$$x(n+1) = A_d x(n) + B_d[u(n) - P_2\text{sign}(\dot{x}(n))] + G_d w(n)$$
$$y(n) = C_d x(n) + v(n)$$

$$A_d = \begin{bmatrix} 1 & T_s \\ 0 & 1 \end{bmatrix} \quad B_d = G_d = \frac{1}{P_1} \times \begin{bmatrix} T_s^2 \\ T_s \end{bmatrix} \quad C_d = [1 \;\; 0]$$

To estimate one sampling step ahead the observation update will be according to equation (6.54) of Kok (1985):

$$\hat{x}(n+1) = A_d\hat{x}(n) + B_d[u(n) - P_2 sign(\dot{x}(n))] + K(y(n) - C_d\hat{x}(n))$$

with the optimum gain matrix K^o according to equation (6.69) of Kok (1985):

$$K^o = A_d\tilde{Q}C_d^T[V_v + C_d\tilde{Q}C_d^T]^{-1}$$

This equation is only mentioned to see the difference with MATLAB, without explaining derivation and symbols. This optimal gain matrix is calculated with function *dlqe* of the software package MATLAB. Because of another updating method, this function calculates an other solution:

$$\text{dlqe}(A_d, G_d, C_d, Q, R) = \tilde{Q}C_d^T[V_v + C_d\tilde{Q}C_d^T]^{-1}$$

which results in:

$$K^o = A_d \times \text{dlqe}(A_d, G_d, C_d, Q, R)$$

with:

$Q = \text{covariance}(w)$
$R = \text{covariance}(v)$

The next step is to determine the covariances Q and R. The measurement noise is determined by the measurement inaccuracy due to incremental encoders. To be safe this inaccuracy is multiplied with factor two. The process noise is determined by experiment. After the experiment the real speed can be determined using a central difference scheme. When the applied input force is used as input for the discrete time model with friction, the position and speed of this model are different from the measured position and speed. An input force is calculated such that the discrete time model with friction follows the measured speed exactly. This is simply done by calculating the acceleration needed to follow the change of speed between two successive samples. Therefore it is always possible to consider the process noise as a disturbance of the input force. Then the difference between this calculated input force and the actually applied input force is the process noise. The covariances of process and measurement noise are:

$Q = 3.0\times10^{8}$ [N^2]

$R = 3.5\times10^{-6}$ [mm^2]

With MATLAB is calculated:

$$K_x^o = A_d \times \begin{bmatrix} 1 \\ 207 \end{bmatrix}$$

with the estimation error covariances of:

position: 3.4×10^{-6} [mm^2]

speed: 8.0 [mm^2/s^2]

In y–direction it goes exactly the same way. The covariances of process and measurement noise are:

$Q = 1.3\times10^{7}$ [N^2]

$R = 8.4\times10^{-5}$ [mm^2]

With MATLAB is calculated:

$$K_y^o = A_d \times \begin{bmatrix} 0.9 \\ 140 \end{bmatrix}$$

with the estimation error covariances of:

position: 1.3×10^{-3} [mm^2]

speed: 46.0 [mm^2/s^2]

But simulations afterwards showed better results with:

$$K_y^o = A_d \times \begin{bmatrix} 0.6 \\ 140 \end{bmatrix}$$

APPENDIX F: ADAPTIVE CONTROLLER DESIGN FOR XY–TABLE

In this appendix the adaptive controller is designed according to chapter 2 for the actual XY–table of chapter 5.

System:

$$H(q)\ddot{q} + w(\dot{q}) = \tau$$

Control law:

$$\tau = \hat{H}(q)\ddot{q}_r + \hat{w}(q) - K_d s$$

$$\tau = Y(q,\dot{q},\dot{q}_r,\ddot{q}_r)\hat{a} - K_d s \qquad (2.3)$$

Adaptation law:

$$\dot{\hat{a}} = -\Gamma^{-1} Y^T(q,\dot{q},\dot{q}_r,\ddot{q}_r)s \qquad (2.4)$$

This yields for XY–table with dynamic equations (5.1):

$$H = \begin{bmatrix} P_1 & 0 \\ 0 & P_2 \end{bmatrix} \quad w = \begin{bmatrix} P_3 \mathrm{sign}(\dot{x}) \\ P_4 \mathrm{sign}(\dot{y}) \end{bmatrix}$$

$$\tau = \begin{bmatrix} F_1 \\ F_3 \end{bmatrix} \quad q = \begin{bmatrix} x \\ y \end{bmatrix} \quad a^T = [P_1\ P_2\ P_3\ P_4]$$

$$Y = \begin{bmatrix} \ddot{x}_r & 0 & \mathrm{sign}(\dot{x}) & \\ 0 & \ddot{y}_r & 0 & \mathrm{sign}(\dot{y}) \end{bmatrix} \qquad (F.1)$$

In paragraph 5.5 the PD controller is designed to create eigenfrequencies of $4\times 2\pi$ [rad/s] and damping factor 0.70 as in equations (5.17). The poles are determined by using the simplified model of equations (5.1). The controlled system is linearized around a point at the desired trajectory of equations (5.18) at t = 0.01 [s]. At this point of time the desired speed is not zero anymore to examine the maximum influence of adaptation of friction parameters, but the desired acceleration is still almost maximum to examine the maximum influence of adaptation of mass parameters. This point of time shows the maximum influences of the adaptation. Because of the simplified model the x– and y–direction can be examined separately. Only PD feedback results in poles:

$$\text{X: PD feedback} \begin{bmatrix} -17.59 + 17.95j \\ -17.59 - 17.95j \end{bmatrix}$$

$$\text{Y: PD feedback} \begin{bmatrix} -17.59 + 17.95j \\ -17.59 - 17.95j \end{bmatrix}$$

This could be expected because:

$$\begin{aligned} &\omega_0 = 4{\times}2\pi \text{ [rad/s]} \\ &\beta = 0.70 \text{ [–]} \end{aligned} \qquad (5.17)$$

$$-\beta\omega_0 \pm \omega_0\sqrt{\beta^2 - 1} = -17.59 \pm 17.95j$$

The adaptive controller with hundred percent parameters but no adaptation results in:

$$\text{X: Adaptation off} \begin{bmatrix} -17.95 \\ -35.19 \\ 0 \\ 0 \end{bmatrix} \begin{matrix} \} \text{ control poles} \\ \\ \} \text{ adaptation poles} \end{matrix}$$

$$\text{Y: Adaptation off} \begin{bmatrix} -17.95 \\ -35.19 \\ 0 \\ 0 \end{bmatrix} \begin{matrix} \} \text{ control poles} \\ \\ \} \text{ adaptation poles} \end{matrix}$$

The extra zero poles are from the adaptation of mass and friction, which is still off. The two non zero poles are equivalent with:

$$\begin{aligned} &\omega_0 = 4{\times}2\pi \text{ [rad/s]} \\ &\beta = 1.06 \end{aligned}$$

which means that the eigenfrequency has stayed exactly the same as in equations (5.17), but the damping factor has become larger. A larger damping factor means a slower system. The bandwidth of the adaptive controller with adaptation off will not be larger than the bandwidth of the PD controller. Until now the adaptation values were always determined small enough not to increase the bandwidth. But to achieve smoothly converging parameters it is much more sensible to choose the adaptation values such that the extra poles due to adaptation and the influence on the existing poles are small. The adaptation values of the matrix Γ^{-1} (chosen diagonal) are:

Γ_{11}^{-1} : adaptation value of mass parameter in x–direction P_1
Γ_{22}^{-1} : adaptation value of mass parameter in y–direction P_2
Γ_{33}^{-1} : adaptation value of friction parameter in x–direction P_3
Γ_{44}^{-1} : adaptation value of friction parameter in y–direction P_4

The adaptation values in x–direction will be increased in steps of factor ten until the adaptation poles and the influence on the control poles become too large.

$$\text{X: } \Gamma_{11}^{-1} = 10^{-3} \begin{bmatrix} -17.95 \\ -33.79 \\ -1.39 \\ 0 \end{bmatrix} \begin{matrix} \} \text{ control poles} \\ \\ \} \text{ adaptation poles} \end{matrix}$$

$$\text{X: } \Gamma_{11}^{-1} = 10^{-2} \begin{bmatrix} -17.95 \\ -17.59 + 12.70j \\ -17.59 - 12.70j \\ 0 \end{bmatrix} \begin{matrix} \} \text{ control poles} \\ \\ \} \text{ adaptation poles} \end{matrix}$$

It is clear that adaptation value 10^{-2} results in a too large adaptation pole and in too large influence on one of the the control poles. Adaptation value 10^{-3} results in a relatively small adaptation pole. The same is done for the other adaptation values:

$$\text{X: } \Gamma_{33}^{-1} = 10^{3} \begin{bmatrix} -17.95 \\ -34.56 \\ -0.62 \\ 0 \end{bmatrix} \begin{matrix} \} \text{ control poles} \\ \\ \} \text{ adaptation poles} \end{matrix}$$

The combined influence in x–direction is:

$$\text{X: } \Gamma_{11}^{-1} = 10^{-3}\,,\ \Gamma_{33}^{-1} = 10^{3} \begin{bmatrix} -17.95 \\ -33.11 \\ -2.07 \\ 0 \end{bmatrix} \begin{matrix} \} \text{ control poles} \\ \\ \} \text{ adaptation poles} \end{matrix}$$

In y–direction:

$$\text{Y: } \Gamma_{22}^{-1} = 10^{-4} \begin{bmatrix} -17.95 \\ -33.67 \\ -1.51 \\ 0 \end{bmatrix} \begin{matrix} \} \text{ control poles} \\ \\ \} \text{ adaptation poles} \end{matrix}$$

$$\text{Y: } \Gamma_{44}^{-1} = 10^{2} \begin{bmatrix} -17.95 \\ -34.51 \\ -0.67 \\ 0 \end{bmatrix} \begin{matrix} \} \text{ control poles} \\ \\ \} \text{ adaptation poles} \end{matrix}$$

The combined influence in y–direction:

$$\text{Y: } \Gamma_{22}^{-1} = 10^{-4}\ \ \Gamma_{44}^{-1} = 10^{2} \begin{bmatrix} -17.95 \\ -32.93 \\ -2.25 \\ 0 \end{bmatrix} \begin{matrix} \} \text{ control poles} \\ \\ \} \text{ adaptation poles} \end{matrix}$$

Because the controlled system with non–linear adaptation law is linearized, the differential equations are dependent. There is always one pole with value zero. But global asymptotic stability of the non linearized system is assured by the adaptive controller itself, which is based on a derivative of the manipulator's total energy smaller or equal to zero. This of course is only valid as long as unmodelled dynamics are not excited. The adaptation values:

$$\Gamma^{-1} = \begin{bmatrix} 10^{-3} & 0 & 0 & 0 \\ 0 & 10^{-4} & 0 & 0 \\ 0 & 0 & 10^{3} & 0 \\ 0 & 0 & 0 & 10^{4} \end{bmatrix} \qquad \text{(F.2)}$$

result in very good parameter estimates as can be seen in chapter 5. The conclusion is that the adaptation values can be determined with a simplified model. The poles have to be determined via linearization of this controlled model. The adaptation values are found quickly by increasing these values with large steps (factor ten). The suitable adaptation values are the values at which the adaptation poles and the influence on the control poles are small.

REFERENCES

1. **Slotine, J. J. E. and W. Li**
Adaptive manipulator control:
A case study
I.E.E.E Int. Conf. Robotics and Automation, vol. 3, 1987

2. **Heeren, T. A. G.**
On control of manipulators
Thesis, Eindhoven University of Technology, 1989

3. **Kok, J. J.**
Werktuigkundig regelen 2
Lecture notes 4594, Eindhoven, 1985

4. **Slotine, J. J. E. and W. Li**
Adaptive manipulator control:
Parameter convergence and task–space strategies
American Control Conference, vol. 2, 1987